Monthly Notices of the ROYAL ASTRONOMICAL SOCIETY

Mon. Not. R. Astron. Soc. **421,** 1298–1314 (2012) doi:10.1111/j.1365-2966.2011.20393.x

The ATLAS^{3D} project – XI. Dense molecular gas properties of CO-luminous early-type galaxies★

Alison Crocker,[1]† Melanie Krips,[2] Martin Bureau,[3] Lisa M. Young,[4] Timothy A. Davis,[3] Estelle Bayet,[3] Katherine Alatalo,[5] Leo Blitz,[5] Maxime Bois,[6,7] Frédéric Bournaud,[8] Michele Cappellari,[3] Roger L. Davies,[3] P. T. de Zeeuw,[6,9] Pierre-Alain Duc,[8] Eric Emsellem,[6,7] Sadegh Khochfar,[10] Davor Krajnović,[6] Harald Kuntschner,[11] Pierre-Yves Lablanche,[6,7] Richard M. McDermid,[12] Raffaella Morganti,[13,14] Thorsten Naab,[15] Tom Oosterloo,[13,14] Marc Sarzi,[16] Nicholas Scott,[17] Paolo Serra[13] and Anne-Marie Weijmans[18]‡

[1]*Department of Astronomy, University of Massachusetts, Amherst, MA 01003, USA*
[2]*Institut de Radio Astronomie Millimétrique (IRAM), Domaine Universitaire, 300 rue de la Piscine, 38406 Saint Martin d'Hères, France*
[3]*Sub-department of Astrophysics, Department of Physics, University of Oxford, Denys Wilkinson Building, Keble Road, Oxford OX1 3RH*
[4]*Department of Physics, New Mexico Institute of Mining and Technology, Socorro, NM 87801, USA*
[5]*Department of Astronomy, University of California, Campbell Hall, Berkeley, CA 94720, USA*
[6]*European Southern Observatory, Karl-Schwarzschild-Str. 2, 85748 Garching, Germany*
[7]*Université Lyon 1, Observatoire de Lyon, Centre de Recherche Astrophysique de Lyon and Ecole Normale Supérieure de Lyon, 9 Avenue Charles André, F-69230 Saint-Genis Laval, France*
[8]*Laboratoire AIM Paris-Saclay, CEA/IRFU/SAp – CNRS – Université Paris Diderot, 91191 Gif-sur-Yvette Cedex, France*
[9]*Sterrewacht Leiden, Leiden University, Postbus 9513, 2300 RA Leiden, the Netherlands*
[10]*Max-Planck Institut für Extraterrestrische Physik, PO Box 1312, D-85478 Garching, Germany*
[11]*Space Telescope European Coordinating Facility, European Southern Observatory, Karl-Schwarzschild-Str. 2, 85748 Garching, Germany*
[12]*Gemini Observatory, Northern Operations Centre, 670 N. A'ohoku Place, Hilo, HI 96720, USA*
[13]*Netherlands Institute for Radio Astronomy (ASTRON), Postbus 2, 7990 AA Dwingeloo, the Netherlands*
[14]*Kapteyn Astronomical Institute, University of Groningen, Postbus 800, 9700 AV Groningen, the Netherlands*
[15]*Max-Planck-Institut für Astrophysik, Karl-Schwarzschild-Str. 1, 85741 Garching, Germany*
[16]*Centre for Astrophysics Research, University of Hertfordshire, Hatfield, Herts AL1 9AB*
[17]*Centre for Astrophysics and Supercomputing, Swinburne University of Technology, PO Box 218, Hawthorn, VIC 3122, Australia*
[18]*Dunlap Institute for Astronomy and Astrophysics, University of Toronto, 50 St George Street, Toronto, ON M5S 3H4, Canada*

Accepted 2011 December 14. Received 2011 December 14; in original form 2011 September 19

ABSTRACT

Surveying 18 ^{12}CO-bright galaxies from the ATLAS^{3D} early-type galaxy sample with the Institut de Radio Astronomie Millimétrique (IRAM) 30-m telescope, we detect ^{13}CO(1–0) and ^{13}CO(2–1) in all 18 galaxies, HCN(1–0) in 12/18 and HCO$^+$(1–0) in 10/18. We find that the line ratios ^{12}CO(1–0)/^{13}CO(1–0) and ^{12}CO(1–0)/HCN(1–0) are clearly correlated with several galaxy properties: total stellar mass, luminosity-weighted mean stellar age, molecular-to-atomic gas ratio, dust temperature and dust morphology. We suggest that these correlations are primarily governed by the optical depth in the ^{12}CO lines; interacting, accreting and/or starbursting early-type galaxies have more optically thin molecular gas while those with settled dust and gas discs host optically thick molecular gas. The ranges of the integrated line intensity ratios generally overlap with those of spirals, although we note some outliers in the ^{12}CO(1–0)/^{13}CO(1–0), ^{12}CO(2–1)/^{13}CO(2–1) and HCN/HCO$^+$(1–0) ratios. In particular, three galaxies are found to have very low ^{12}CO(1–0)/^{13}CO(1–0) and ^{12}CO(2–1)/^{13}CO(2–1) ratios. Such low ratios may signal particularly stable molecular gas which creates stars less

★Based on observations carried out with the IRAM 30-m telescope. IRAM is supported by INSU/CNRS (France), MPG (Germany) and IGN (Spain).
†E-mail: crocker@astro.umass.edu
‡Dunlap fellow.

© 2012 The Authors
Monthly Notices of the Royal Astronomical Society © 2012 RAS

efficiently than 'normal' (i.e. below Schmidt–Kennicutt prediction), consistent with the low dust temperatures seen in these galaxies.

Key words: galaxies: elliptical and lenticular, cD – galaxies: evolution – galaxies: ISM – galaxies: kinematics and dynamics – galaxies: stellar content.

1 INTRODUCTION

Molecular gas is an essential ingredient for star formation found in many, but not all, galaxies. Early-type galaxies (ellipticals and lenticulars) were classically thought to completely lack molecular gas and to be passively evolving 'red and dead' galaxies. However, we have long known that not all early-types are empty of cold gas; molecular gas was first detected in early-type galaxies by Wiklind & Rydbeck (1986) and Phillips et al. (1987).

Shortly after these first detections, surveys detected 10–20 galaxies, but were biased towards early-types with particular properties, such as those bright in the far-infrared (FIR; Wiklind & Henkel 1989; Sage & Wrobel 1989) or with optically obscuring dust (Wang, Kenney & Ishizuki 1992). These selection effects made it easy to dismiss any early-type galaxies with molecular gas as peculiar systems. The next generation of surveys increased numbers (30–50 galaxies) and were less biased, if still not complete (Welch & Sage 2003; Combes, Young & Bureau 2007; Sage, Welch & Young 2007). In Young et al. (2011, hereafter Paper IV), we have recently completed an extensive (259 galaxies) molecular gas detection campaign for the volume-limited ATLAS^{3D} sample of early-type galaxies. We find a 22 per cent detection rate, down to a typical detection threshold of 6×10^7 M$_\odot$ of H_2, robustly establishing that many early-type galaxies host a substantial amount of molecular gas.

The majority of early-type galaxies with molecular gas are obviously star forming, based on ultraviolet (UV), optical or infrared data. Indeed, the detection rate for star formation seen in UV nearly matches the molecular detection rate (≈30 per cent; Kaviraj et al. 2007). According to the current observations, the star formation efficiencies of early-type galaxies broadly follow the Kennicutt–Schmidt law (Shapiro et al. 2010; Crocker et al. 2011). A subset shows no obvious sign of ongoing star formation (Crocker et al. 2008, 2011), although these determinations are difficult due to their very low specific star formation rates. Recently, Saintonge et al. (2011) have determined that star formation efficiencies are reduced for more massive, more concentrated and higher stellar surface density galaxies, all properties that positively correlate with early-type morphology.

In a spiral galaxy, the presence of a stellar disc renders the gas disc more locally unstable to axisymmetric perturbations, likely boosting its star formation efficiency (e.g. Jog & Solomon 1984). In Krajnović et al. (2011, hereafter Paper II) and Emsellem et al. (2011, hereafter Paper III), we found that the vast majority of early-type galaxies (the fast rotators) are consistent with being a family of disc-like systems resembling spiral galaxies with the gas and dust removed (Cappellari et al. 2011b, hereafter Paper VII). However, the fast rotators are generally characterized by larger spheroids than spiral galaxies. This increase in the depth of the potential well is expected to make their gas discs more stable against fragmentation (Kawata, Cen & Ho 2007).

Indeed, simulations with a centrally concentrated stellar mass distribution (as found in spheroids) and no stellar disc show that the cool gas is more stable than in spiral galaxies (Martig et al. 2009). This stability (termed 'morphological quenching') should lower the efficiency of star formation and produce a cool interstellar medium (ISM) with properties (velocity dispersion, density distribution, etc.) different from those of galaxies with stellar discs. In this paper, we present the first major attempt at constraining the empirical properties of the molecular gas in early-type galaxies, especially looking for any divergence from the properties found for spiral galaxies.

The surveys mentioned above have used the bright ^{12}CO(1–0) emission line to measure the total molecular content of early-type galaxies, but little work has been done to constrain the molecular gas properties using other species and transitions. Several other molecular species are bright enough to measure, including ^{13}CO, HCN and HCO$^+$. These species have been widely observed in starburst and Seyfert galaxies and also in some local spiral galaxies.

The observed ^{12}CO/^{13}CO ratio is widely used to indicate the average optical depth of the molecular gas,[1] although it may also be influenced by chemical processes. The ^{12}CO isotope is far more abundant and becomes optically thick at lower H_2 column densities. Its use as a measure of the total molecular hydrogen content (via one of the ^{12}CO-to-H_2 conversion factors X_{CO} or α_{CO}) relies on the assumption that it is optically thick, and essentially counts the number of virialized molecular clouds of a similar temperature and density (e.g. Young & Scoville 1991). The less abundant ^{13}CO isotope is optically thin until higher column densities and thus the ^{12}CO/^{13}CO ratio (often denoted $\mathfrak{R}$) should reflect differences in average optical depth in ^{12}CO, either within the molecular clouds themselves or because of the additional contribution of a diffuse molecular component. Variations in the ^{12}C to ^{13}C abundance ratio and ^{12}CO ↔ ^{13}CO fractionation (due to charge–ion reactions or selective photodissociation) must also be considered, although they do not seem to drive this ratio in spiral galaxies (Paglione et al. 2001).

The HCN(1–0) and HCO$^+$(1–0) lines have higher critical densities (approximately 10^6 and 10^5 cm^{-3}, respectively) than CO(1−0) ($n_{\rm crit} \approx 10^3$).[2] The critical density is simply the density at which collisions are more frequent than radiative decays, not a strict limit with no emission at lower densities. Thus, depending on the density distribution of the molecular gas, the typical gas density probed by the HCN(1–0) and HCO$^+$(1–0) transitions will vary from system to system, although in all cases it will be higher than the densities probed by CO(1–0).

Higher HCN/^{12}CO and HCO$^+$/^{12}CO ratios in luminous infrared galaxies (LIRGs) and ultra-luminous infrared galaxies (ULIRGs) are thus taken to indicate higher dense gas fractions in these galaxies (Gao & Solomon 2004a; Graciá-Carpio et al. 2006). The more moderate increase of HCO$^+$/^{12}CO compared to HCN/^{12}CO in these

[1] Described by $(^{12}\mathrm{CO}/^{13}\mathrm{CO})_{\rm obs} = [\mathrm{e}^{-\tau(12)}/\mathrm{e}^{-\tau(13)}](^{12}\mathrm{CO}/^{13}\mathrm{CO})$.

[2] Note that effective critical densities, which take into account radiative trapping, are about an order of magnitude lower (e.g. Scoville & Solomon 1974).

© 2012 The Authors, MNRAS **421,** 1298–1314
Monthly Notices of the Royal Astronomical Society © 2012 RAS

systems may be explained by the order of magnitude difference in the critical densities of HCN(1–0) and HCO^+(1–0) (Juneau et al. 2009). In both the Milky Way and M31, the HCN/^{12}CO ratio declines with radius, signalling the decline of the dense gas content (Helfer & Blitz 1997; Brouillet et al. 2005). Indeed, Helfer & Blitz (1997) find that the HCN(1–0)/^{12}CO(1–0) ratio correlates with the hydrostatic pressure in the disc: HCN(1–0)/^{12}CO(1–0) $\propto P^{0.19\ \pm 0.04}$.

Molecular chemistry can also influence the HCN and HCO^+ emission seen in galaxies. X-ray-dominated regions (XDRs) around active galactic nuclei (AGN) may enhance the HCN abundance relative to CO (e.g. Lepp & Dalgarno 1996). This effect has been observed in Seyfert galaxies and led to the recommendation to prefer HCO^+ as a dense gas tracer (Graciá-Carpio et al. 2006; Krips et al. 2007). However, Papadopoulos (2007) warn about possible effects of free electrons in cosmic-ray-dominated regions (CRDRs) and XDRs, or highly turbulent molecular clouds destroying HCO^+. Nevertheless, most of these chemical effects rely on the conditions found in starbursts or AGN, and hence HCN and HCO^+ are likely to remain good tracers of dense gas in more quiescent regimes.

Until recently, the only early-type galaxy to be studied in molecular species other than ^{12}CO was Centaurus A (Cen A), with its striking lane of dust and gas. The $\approx 5 \times 10^8$ M$_\odot$ of molecular gas in its disc extends to about 2.6 kpc (Phillips et al. 1987; Eckart et al. 1990), while 4×10^8 M$_\odot$ of atomic gas is seen in a warped disc out to about 6 kpc (van Gorkom et al. 1990; Struve et al. 2010). While often considered a galaxy completely in its own class, its molecular and atomic gas content is not very different from that of some of our sample galaxies. In terms of molecular emission line studies, Wild, Eckart & Wiklind (1997) found a ^{12}CO(1–0)/^{13}CO(1–0) ratio of 14 towards the centre of Cen A and 11 towards two positions in its disc, similar values as found in spirals. As for HCN, Wild & Eckart (2000) find a higher ratio of HCN(1–0)/^{12}CO(1–0) in the centre (0.067) than in offset positions along the disc (0.02–0.04).

In Krips et al. (2010), the ^{13}CO(1–0),^{13}CO(2–1), HCN(1–0) and HCO^+(1–0) emission lines of four early-type galaxies were measured as a pilot project for this work. Two of these galaxies have particularly low ^{12}CO(1–0)/^{13}CO(1–0) ratios of around 3 and two have more typical ratios of around 10. The HCN(1–0)/^{13}CO(1–0) and HCN(1–0)/^{12}CO(1–0) ratios are in the range observed for spiral and Seyfert galaxies, but lower than those for starbursts. Most curiously, none were detected in HCO^+(1–0), despite 3/4 being detected in HCN(1–0), which usually has a similar integrated intensity. In one case, the HCN(1–0)/HCO^+(1–0) ratio is constrained to be larger than 2, indicating some significant difference in the chemistry or physical properties of this galaxy's molecular gas compared to those of spiral, Seyfert and starburst galaxies.

In this paper, we extend the original sample of four early-type galaxies from Krips et al. (2010) to a sample of 18 galaxies from the ATLAS^{3D} sample. Section 2 describes the sample selection and Section 3 describes our observations and data reduction. We compare the profiles of the different molecular lines within each galaxy and discuss the derived line ratios in Section 4. In Section 4, we also investigate the variations of the molecular line ratios with other galaxy properties. Our conclusions are presented in Section 5.

2 SAMPLE

We draw our sample from the ^{12}CO(1–0) detections of Paper IV which presents ^{12}CO(1–0) data on 259 of the 260 early-type galaxies in the ATLAS^{3D} sample. The ATLAS^{3D} sample is volume-limited and complete to a distance $D < 42$ Mpc, with a cut-off absolute magnitude of $M_K = -21.5$. It includes only early-type galaxies, defined according to classic galaxy morphology (Hubble 1936; Sandage 1961) by the absence of spiral arms (for non-edge-on galaxies) or by the lack of galaxy-scale dust lanes (for edge-on galaxies). Further details on the sample can be found in Cappellari et al. (2011a, hereafter Paper I).

Paper IV detects ^{12}CO in 56/259 of the ATLAS^{3D} sample galaxies, based on centrally pointed observations using the Institut de Radio Astronomie Millimétrique (IRAM) 30-m telescope. An rms noise of around 3.0 mK (T_A^*) in ^{12}CO(1–0) was achieved for every galaxy. With a conversion factor of $X_{CO} = 3.0 \times 10^{20}$ cm^{-2} (K km s^{-1})$^{-1}$, this results in a molecular gas mass detection limit of 1×10^7 M$_\odot$ for the nearest sample galaxies (11 Mpc) and 1×10^8 M$_\odot$ for the furthest sample galaxies (40 Mpc). Due to the expected lower intensity of the ^{13}CO(1–0), ^{13}CO(2–1), HCN(1–0) and HCO^+(1–0) lines, we selected the 18 strongest ^{12}CO(1–0) detections for follow-up at these transitions. Both peak brightness temperature and line width were used to determine the 'strength' of the ^{12}CO(1–0) detections. Out of these 18 galaxies, four were previously observed and reported in the Krips et al. (2010) pilot study. Details of the sample galaxies are provided in Table 1, including the H_2 mass derived in Paper IV.

The necessity of choosing the brightest ^{12}CO(1–0) detections biases our sample towards galaxies with large molecular gas masses and large molecular gas mass fractions, as can be seen in the top panel of Fig. 1. However, using Kolmogorov–Smirnov tests, the 18 galaxies selected are consistent with being a randomly drawn subsample of both the remainder of the CO-detected galaxies and the non-CO-detected ATLAS^{3D} galaxies, with respect to the distribution of their absolute K-band magnitude, Σ_3 (a measure of local environment density; see Paper VII) and λ_R (a measure of the stellar-specific angular momentum used to classify galaxies as fast or slow rotators; see Paper III). The distributions of these three parameters are plotted in the bottom panel of Fig. 1. The selected subsample is slightly biased with respect to dust temperature (indicated by the f_{60}/f_{100} ratio) when compared to the other CO detections (top panel of Fig. 1). The probability that the two distributions are drawn from the same parent population is only 1.1 per cent, the CO-rich subsample being biased towards higher dust temperatures, but also possibly being more narrowly spread than the other CO detections.

3 IRAM 30-m OBSERVATIONS AND DATA REDUCTION

We used the IRAM 30-m telescope at Pico Veleta, Spain, to observe the ^{13}CO(1–0), ^{13}CO(2–1), HCN(1-0) and HCO^+(1–0) transitions in 2009 July and 2010 April. The Eight Mixer Receiver (EMIR) was used, tuned to either the ^{13}CO(1–0) or HCN(1–0) redshifted frequency at 3 mm and simultaneously to ^{13}CO(2–1) at 1 mm for both 3-mm set-ups. The rest frequencies and beam sizes for each of the lines are specified in Table 2. We observed in wobbler-switching mode with reference position offsets of ± 120 arcsec. The Wideband Line Multiple Autocorrelator (WILMA) back-end provided a bandwidth of 8 GHz at 2-MHz channel resolution [2 MHz corresponds to 6.7, 5.5 and 2.7 km s^{-1} at ^{13}CO(1–0), HCN(1–0) and ^{13}CO(2–1), respectively]. This bandwidth is sufficient to observe HCO^+(1–0) and HCN(1–0) simultaneously.

System temperatures ranged from 90 to 200 K at 3 mm and 250 to 600 K at 1 mm. The pointing was checked approximately every 2–3 h or more frequently during periods of high wind. Focusing was performed at the beginning of the night, after sunrise or sunset, and/or after about 5–6 h of observing.

Table 1. Sample properties.

Name	D (Mpc)	M_K (mag)	λ_{R_e}	ϵ_e	ρ_{10} (Mpc^{-3})	log(M_{HI}) (M$_\odot$)	log(M_{H_2}) (M$_\odot$)	f_{60}/f_{100}	Dust morphology	[O III]/Hβ
IC 0676	24.6	−22.27	0.49	0.524	−1.41	8.27[a]	8.62	0.62	F	0.32
IC 1024	24.2	−21.85	0.72	0.679	−0.85	9.04[b]	8.57	0.52	F	0.60
NGC 1222	33.3	−22.71	0.15	0.280	−1.90	9.31[b]	9.08	0.85	F	1.81
NGC 1266	29.9	−22.93	0.64	0.193	−2.11	6.98[c]	9.29	0.79	F	1.70
NGC 2764	39.6	−23.19	0.66	0.614	−2.01	9.28	9.19	0.51	F	0.44
NGC 3032	21.4	−22.01	0.34	0.102	−1.52	8.04	8.41	0.41	D	0.31
NGC 3607	22.2	−24.74	0.21	0.185	−0.92	<6.92	8.42	–	D	0.99
NGC 3665	33.1	−24.94	0.41	0.216	−1.94	<7.43	8.91	0.25	D	0.61
NGC 4150	13.4	−21.65	0.51	0.328	−1.18	6.26	7.82	0.46	N	1.53
NGC 4459	16.1	−23.89	0.44	0.148	0.78	<6.91	8.24	0.39	D	0.66
NGC 4526	16.4	−24.62	0.45	0.361	0.83	<7.68[d]	8.59	0.33	D	0.81
NGC 4694	16.5	−22.15	0.29	0.547	0.60	8.21	7.99	0.41	F	0.68
NGC 4710	16.5	−23.53	0.65	0.699	0.09	6.84	8.69	0.39	D	1.13
NGC 5866	14.9	−24.00	0.32	0.566	−2.12	6.96	8.47	0.27	D	–
NGC 6014	35.8	−22.99	0.39	0.419	−2.27	<8.28[a]	8.80	0.63	D	0.45
NGC 7465	29.3	−22.82	0.28	0.364	−1.97	9.98	8.80	0.47	F	0.87
PGC 058114	23.8	−21.57	0.18	0.185	−2.31	8.23[e]	8.61	0.78	–	0.64
UGC 09519	27.6	−21.98	0.63	0.484	−2.41	9.27	8.80	0.40	F	1.14

Note. Distances and M_K from Paper I; λ_{R_e} and ϵ_e from Paper III; ρ_{10} from Paper VII; H I content from Serra et al. (2012); H_2 content from Paper IV; f_{60}/f_{100} derived from *IRAS* measurements; dust morphology is D for disc, F for filamentary and N for none from Paper II. Exceptions: [a]Grossi et al. (2009), [b]Paturel et al. (2003), [c]Alatalo et al. (2011), [d]Knapp, Kerr & Henderson (1979) and [e]Springob et al. (2005).

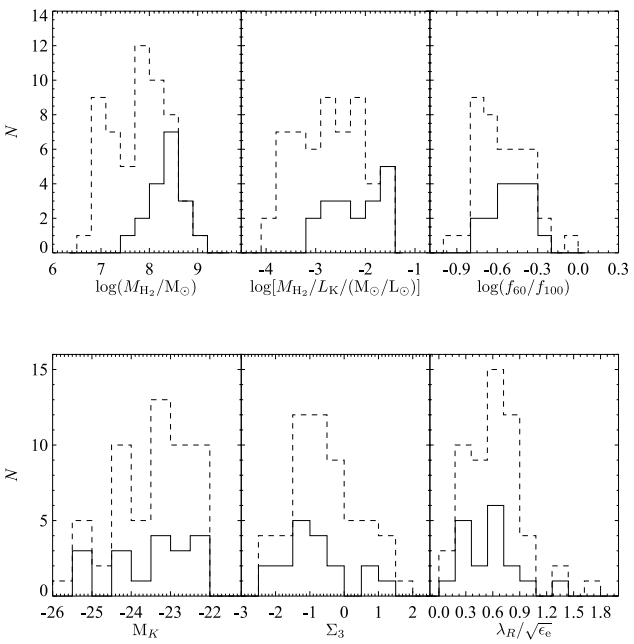

Figure 1. Distributions of the 56 galaxies selected for follow-up (solid lines) out of the 59 ^{12}CO(1–0) detections from ATLAS^{3D} (dashed lines). Top panel: our subsample is clearly biased towards the highest molecular gas masses and mass fractions and slightly biased towards warmer dust temperatures, as measured by the *Infrared Astronomical Satellite* (*IRAS*) 60–100 μm flux ratio (f_{60}/f_{100}). The bottom panel shows no bias in absolute K-band magnitude, local environment (Σ_3) or specific stellar angular momentum ($\lambda_R/\sqrt{\epsilon_e}$).

Observations for four sample galaxies (NGC 3032, NGC 4150, NGC 4459 and NGC 4526) were taken in 2008 August and published in Krips et al. (2010). We note that these observations used the old SIS receiver and thus a different observing set-up than the other 14 galaxies. Observing details are described in Krips et al. (2010).

Table 2. Observed line frequencies and beam sizes.

Line	Rest frequency (GHz)	Beam size (arcsec)
HCN(1–0)	88.632	27.7
HCO$^+$(1–0)	89.189	27.7
^{13}CO(1–0)	110.201	22.3
^{13}CO(2–1)	220.399	11.2

Conversions from antenna temperature (T_A^*) to main beam temperature were calculated by dividing by the ratio of the beam and forward efficiencies, $\eta \equiv B_{eff}/F_{eff}$. We used values appropriate for when the observations were taken. For the new observations, values tabulated in the EMIR Commissioning Report[3] were used. To obtain B_{eff} and F_{eff} values at frequencies not specified in these tables, we linearly interpolated between the two nearest values. The conversion ratios used for the new observations are: η(HCN) = η(HCO$^+$) = 0.85, η[^{13}CO(1–0)] = 0.83 and η[^{13}CO(2–1)] = 0.66. For the older observations, we base our conversions on the measurements performed in 2007 August and 2008 June. For the 1-mm values, linear interpolation is again used. However, noting the discrepant values found for the C150 receiver, we follow the approach of Paper IV for the 3-mm values. The 3-mm B_{eff} values are based on the aperture efficiency plot on page 15 of the IRAM 2007 Annual Report[4] ($B_{eff} = 1.21A_{eff}$, where A_{eff} is the aperture efficiency). This results in η(HCN) = η(HCO$^+$) = 0.79, η[^{13}CO(1–0)] = 0.78, η[^{12}CO(1–0)] = 0.78, η[^{13}CO(2–1)] = 0.65 and η[^{12}CO(2–1)] = 0.63.

[3] http://www.iram.es/IRAMES/mainWiki/EmirforAstronomers
[4] http://www.iram.fr/IRAMFR/ARN/AnnualReports/IRAM_2007.pdf

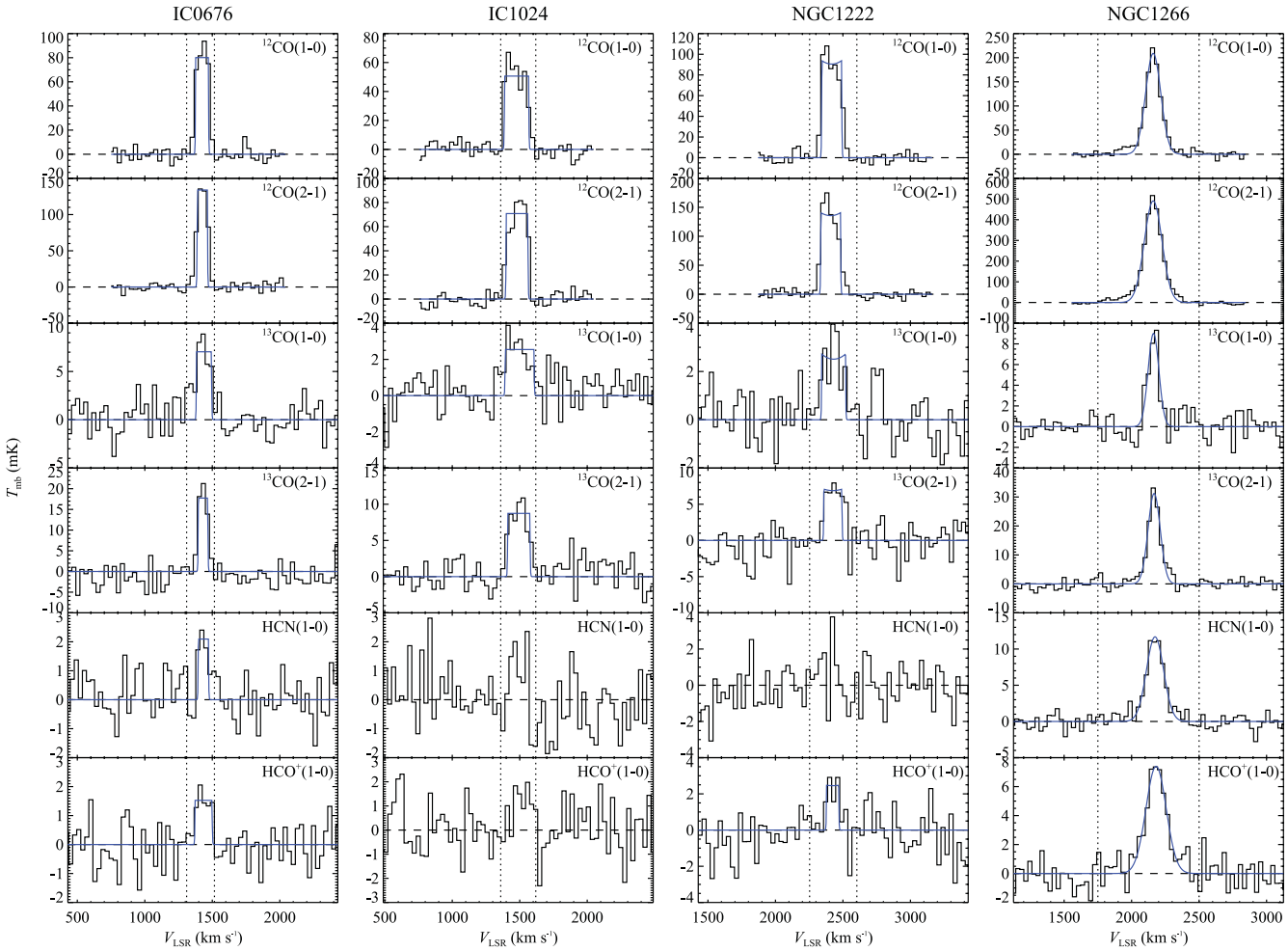

Figure 2. Example molecular line spectra from the IRAM 30-m telescope; spectra of the remaining 14 galaxies are shown in Appendix A. The spectra have been binned to a channel width of 30 km s^{-1} and the scale is in main beam temperature (mK). The blue line shows the best-fitting Gaussian or double-peak function (fits are only performed on detected lines). The vertical dashed lines indicate the velocity range integrated over to obtain integrated intensities. Top to bottom: ^{12}CO(1–0), ^{12}CO(2–1), ^{13}CO(1–0), ^{13}CO(2–1), HCN(1–0) and HCO$^+$(1–0). The ^{12}CO(1–0) and ^{12}CO(2–1) data are from Paper IV.

Linear baselines were fitted to frequencies outside of the expected line region for each scan, then the scans were averaged together weighted by their system temperature. The spectra for four sample galaxies are shown in Fig. 2 in the $T_{\rm mb}$ scale, with the rest in Appendix A. The figures include ^{12}CO(1–0) and ^{12}CO(2–1) spectra from Paper IV and Welch & Sage (2003) for comparison.

As all of the galaxies have previous well-measured molecular line widths from the ^{12}CO(1–0) data, and we use this prior knowledge to help ascertain detections and measure integrated intensities. In order for a galaxy to be detected, we require the integrated intensity over its ^{12}CO(1–0)-detected velocity range to be three times greater than the uncertainty expected over such a velocity width. As in Sage et al. (2007) and Paper IV, the statistical uncertainty $\sigma_{\rm I}$ in a sum over $N_{\rm l}$ channels of width δv and rms noise level σ is $\sigma_{\rm I}^2 = (\delta v)^2\sigma^2 N_{\rm l}(1+N_{\rm l}/N_{\rm b})$, where $N_{\rm b}$ is the number of baseline channels used (and thus the $N_{\rm l}/N_{\rm b}$ term contributes the uncertainty from estimating the baseline level). The rms noise is measured outside of the range where line emission is expected. If a galaxy is not detected, we give three times the measured uncertainty as an upper limit. Integrated intensities with errors are tabulated in Table 3, along with the velocity range integrated over. We note that only the measurement errors are tabulated, and systematic uncertainties are also important at around 10 per cent.

4 RESULTS

4.1 Consistency of line profiles

Assuming that the intrinsic velocity dispersion of the molecular gas is low (<30 km s^{-1}, the channel width), the spectral profile of each molecular line is governed by the velocity field of the galaxy coupled with the spatial distribution of the gas emitting in that line. Changes in spectral shape from line to line can indicate different molecular gas properties at different locations within a galaxy. We thus compare the line profiles of each galaxy, testing for consistency as documented in Appendix B. Briefly, we first determine whether a Gaussian or a double-peaked profile is the best fit to the ^{12}CO(1–0) line. Then, using this best-fitting functional form, we determine whether the shape parameters (leaving amplitude free) for all other lines are consistent with those derived for the ^{12}CO(1–0) line.

Three galaxies, NGC 1266, NGC 3607 and NGC 4526, have line profiles inconsistent with ^{12}CO(1–0) for all or almost all of their other lines. For NGC 1266 (best fitted by a Gaussian), the full width at half-maximum (FWHM) is significantly greater in its ^{12}CO(2–1), HCN(1–0) and HCO$^+$(1–0) lines and is significantly narrower in both ^{13}CO lines (further discussed in Section 4.3). Alatalo et al. (2011) find that NGC 1266's ^{12}CO(1–0) and ^{12}CO(2–1) line profiles

Table 3. ^{12}CO(1–0), ^{12}CO(2–1), ^{13}CO(1–0), ^{13}CO(2–1), HCN(1–0) and HCO$^+$(1–0) integrated intensities.

Galaxy	Velocity range (km s^{-1})	^{12}CO(1–0) (K km s^{-1})	^{12}CO(2–1) (K km s^{-1})	^{13}CO(1–0) (K km s^{-1})	^{13}CO(2–1) (K km s^{-1})	HCN(1–0) (K km s^{-1})	HCO$^+$(1–0) (K km s^{-1})
IC 0676	1310–1516	11.46 ± 0.39	16.78 ± 0.32	1.44 ± 0.11	1.97 ± 0.15	0.27 ± 0.06	0.27 ± 0.06
IC 1024	1359–1619	11.41 ± 0.38	15.74 ± 0.36	0.72 ± 0.08	1.90 ± 0.12	<0.27	<0.28
NGC 1222	2253–2603	17.32 ± 0.45	28.95 ± 0.49	0.78 ± 0.10	1.42 ± 0.20	<0.36	0.37 ± 0.12
NGC 1266	1750–2500	34.76 ± 0.99	105.22 ± 0.88	1.04 ± 0.09	4.04 ± 0.19	2.83 ± 0.15	1.97 ± 0.15
NGC 2764	2514–2944	16.17 ± 0.48	24.54 ± 0.71	1.41 ± 0.10	2.01 ± 0.14	0.28 ± 0.08	0.47 ± 0.08
NGC 3032[a]	1475–1630	8.32 ± 0.23	6.61 ± 0.27	0.84 ± 0.07	1.23 ± 0.09	0.27 ± 0.04	<0.33
NGC 3607	670–1227	10.44 ± 0.29	19.54 ± 2.20	1.66 ± 0.17	2.96 ± 0.32	0.73 ± 0.10	0.51 ± 0.10
NGC 3665	1737–2432	11.97 ± 0.64	14.35 ± 0.83	3.71 ± 0.19	5.64 ± 0.19	0.49 ± 0.08	<0.23
NGC 4150[a]	75–350	6.04 ± 0.47	10.99 ± 0.49	0.42 ± 0.07	0.87 ± 0.11	<0.24	<0.25
NGC 4459[a]	980–1385	10.03 ± 0.56	11.52 ± 0.51	2.99 ± 0.13	4.03 ± 0.21	0.59 ± 0.12	<0.62
NGC 4526[a]	280–980	21.63 ± 1.00	32.26 ± 0.89	5.95 ± 0.28	6.76 ± 0.34	1.75 ± 0.12	<0.63
NGC 4694	1083–1264	6.14 ± 0.35	6.60 ± 0.28	0.35 ± 0.08	0.65 ± 0.14	<0.20	<0.20
NGC 4710	896–1368	31.65 ± 0.74	40.42 ± 0.62	4.77 ± 0.15	6.13 ± 0.20	1.41 ± 0.10	0.89 ± 0.10
NGC 5866	432–1051	21.57 ± 0.38	17.35 ± 0.68	3.27 ± 0.16	3.80 ± 0.18	0.84 ± 0.09	0.57 ± 0.09
NGC 6014	2266–2570	7.48 ± 0.38	10.81 ± 0.37	0.78 ± 0.13	1.54 ± 0.10	0.20 ± 0.05	<0.14
NGC 7465	1827–2117	11.89 ± 0.39	21.48 ± 0.43	0.63 ± 0.14	1.15 ± 0.06	0.13 ± 0.03	0.29 ± 0.03
PGC 058114	1383–1768	11.37 ± 0.38	21.65 ± 0.27	0.56 ± 0.09	1.45 ± 0.20	<0.33	0.38 ± 0.11
UGC 09519	1501–1818	12.64 ± 0.38	13.96 ± 0.29	0.45 ± 0.10	0.88 ± 0.18	<0.21	0.29 ± 0.07

[a]Pilot sample galaxies from Krips et al. (2010).

are best fitted by two nested Gaussians (with a shared centre). We thus perform such a nested two-Gaussian fit for the other molecular lines of NGC 1266, but find that the two-Gaussian fit does not result in a significantly lower χ^2 value in these other lines. For NGC 3607 and NGC 4526, the distinct changes in shape are consistent with pointing offsets which preferentially miss one side of their double-peak profiles.

Out of all the galaxies, NGC 5866 has the most interesting diversity of line profiles. Despite an asymmetry likely due to pointing in both ^{12}CO lines, it is clearly double peaked in both ^{12}CO lines, HCN(1–0) and HCO$^+$(1–0), while both ^{13}CO lines show a clear single central peak. In this galaxy, the molecular gas must have different properties in the centre and the disc.

The line most frequently found to be inconsistent with ^{12}CO(1–0) is the ^{12}CO(2–1) line. These two lines have the highest signal-to-noise ratio and thus their parameters are best constrained, making it harder for them to be formally consistent. The different beam sizes (factor 2) means a smaller region is traced in ^{12}CO(2–1), providing one reason for potential line-profile differences along with gas property variations and, additionally, the ^{12}CO(2–1) line is very sensitive to pointing offsets, as clearly seen in NGC 3607, NGC 3665, NGC 4526 and NGC 5866.

At some level, we expect the intrinsic line profiles in the various lines to all be different, due to different local conditions in the molecular gas. Higher signal-to-noise data should show such varying profiles and allow variations in the physical properties of the molecular gas to be studied. However, the relatively low signal-to-noise ratio of our observations does not allow for such detailed work and we thus only consider integrated intensity ratios for the remainder of this paper.

4.2 Line ratio diagnostics

Molecular line ratios are a first step to diagnose the state of the molecular gas within galaxies. Here we compare the line ratios of our early-type galaxies with those of spirals, Seyfert nuclei and starbursts. We also test if the molecular line ratios correlate with other ISM and stellar properties of the galaxies.

We compute the integrated line ratios after using interferometric ^{12}CO(1–0) data (Alatalo et al., in preparation) to estimate beam correction factors for each galaxy. Appendix C tabulates these values and describes the process. This step is necessary, as the transitions we compare are at different frequencies, thus measured over different beam sizes. Corrections from HCN or HCO$^+$ to ^{12}CO(1–0) are up to 60 per cent in the case of the most centrally concentrated sources, but the corrections for most sources range between 30 and 50 per cent. All corrections are under 10 per cent between the ^{12}CO and ^{13}CO lines and no correction is required between HCN(1–0) and HCO$^+$(1–0) as they are very close in frequency.

Errors on the integrated intensity ratios are calculated using a very simple Monte Carlo simulation of errors through division. We include the measurement errors of Table 3 and, for ratios of lines not measured simultaneously (i.e. all except HCN/HCO$^+$), a 10 per cent systematic error contribution. This simulation is necessary because the non-linear operation of division produces a strongly biased (non-Gaussian) error distribution, which is not well approximated by the standard error propagation formula. The bias is particularly noticeable here because our measurements are small compared to their errors (i.e. low signal-to-noise ratio; large relative errors push the first-order Taylor expansion of the standard error propagation formula beyond its region of validity). Using 1000 samples from a Gaussian distribution around each integrated intensity and dividing, we then calculate upper and lower errors by sorting the obtained values and identifying the values that exclude the bottom and top 15.9 per cent (leaving the central 68.2 per cent range of values, thus akin to 1σ errors on a Gaussian distribution).

4.2.1 ^{12}CO/^{13}CO

The sample galaxies vary by a factor of 10 in both ^{12}CO(1–0)/^{13}CO(1–0) (hereafter $\mathfrak{R}_{10}$) and ^{12}CO(2–1)/^{13}CO(2–1) (hereafter $\mathfrak{R}_{21}$; see Table 4) and these two ratios are well correlated (see the top panel of Fig. 3). However, about half the sample galaxies have significantly larger $\mathfrak{R}_{10}$ than $\mathfrak{R}_{21}$ ratios, as can be seen by comparing the galaxies to the solid 1:1 line in Fig. 3 (error bars do not intersect the line). The galaxy area probed by the (1–0) transition

© 2012 The Authors, MNRAS **421,** 1298–1314
Monthly Notices of the Royal Astronomical Society © 2012 RAS

Table 4. Integrated intensity line ratios.

Galaxy	^{12}CO/^{13}CO (1–0)	^{12}CO/^{13}CO (2–1)	HCN/^{12}CO (1–0)	HCN/^{13}CO (1–0)	HCN/HCO$^+$ (1–0)	^{13}CO/HCO$^+$ (1–0)	^{12}CO(1–0)/ ^{12}CO(2–1)
IC 0676	$7.5^{+1.3}_{-1.2}$	$8.3^{+1.4}_{-1.3}$	$0.033^{+0.008}_{-0.008}$	$0.25^{+0.07}_{-0.06}$	$1.00^{+0.35}_{-0.26}$	$4.03^{+1.29}_{-0.92}$	$1.34^{+0.05}_{-0.05}$
IC 1024	$15.1^{+3.0}_{-2.6}$	$8.1^{+1.3}_{-1.2}$	<0.024	<0.38	–	>2.61	$1.17^{+0.05}_{-0.05}$
NGC 1222	$21.1^{+4.5}_{-3.8}$	$20.0^{+4.5}_{-3.7}$	<0.021	<0.46	<0.96	$1.65^{+0.86}_{-0.49}$	$0.98^{+0.03}_{-0.03}$
NGC 1266	$30.9^{+5.6}_{-5.0}$	$24.8^{+3.8}_{-3.6}$	$0.128^{+0.020}_{-0.020}$	$3.94^{+0.73}_{-0.66}$	$1.43^{+0.14}_{-0.13}$	$0.36^{+0.07}_{-0.07}$	$0.86^{+0.03}_{-0.03}$
NGC 2764	$10.8^{+1.8}_{-1.7}$	$11.6^{+1.9}_{-1.8}$	$0.025^{+0.008}_{-0.008}$	$0.27^{+0.08}_{-0.08}$	$0.59^{+0.21}_{-0.17}$	$2.22^{+0.57}_{-0.45}$	$1.50^{+0.06}_{-0.06}$
NGC 3032	$9.5^{+1.6}_{-1.5}$	$5.3^{+0.9}_{-0.8}$	$0.044^{+0.009}_{-0.009}$	$0.41^{+0.09}_{-0.09}$	>0.81	>2.52	$2.04^{+0.11}_{-0.10}$
NGC 3607	$5.9^{+1.1}_{-1.0}$	$6.4^{+1.4}_{-1.3}$	$0.097^{+0.019}_{-0.019}$	$0.58^{+0.13}_{-0.12}$	$1.43^{+0.40}_{-0.29}$	$2.47^{+0.75}_{-0.56}$	$1.03^{+0.13}_{-0.11}$
NGC 3665	$3.0^{+0.5}_{-0.5}$	$2.4^{+0.4}_{-0.4}$	$0.060^{+0.013}_{-0.013}$	$0.18^{+0.04}_{-0.04}$	>2.13	>16.21	$1.93^{+0.16}_{-0.15}$
NGC 4150	$13.7^{+3.6}_{-2.9}$	$12.2^{+2.7}_{-2.2}$	<0.040	<0.58	–	>1.71	$1.08^{+0.10}_{-0.09}$
NGC 4459	$3.2^{+0.5}_{-0.5}$	$2.8^{+0.4}_{-0.4}$	$0.081^{+0.020}_{-0.020}$	$0.26^{+0.06}_{-0.06}$	>0.95	>4.80	$1.39^{+0.10}_{-0.10}$
NGC 4526	$3.5^{+0.5}_{-0.5}$	$4.6^{+0.7}_{-0.7}$	$0.108^{+0.018}_{-0.017}$	$0.38^{+0.06}_{-0.06}$	>2.77	>9.41	$1.15^{+0.06}_{-0.06}$
NGC 4694	$16.6^{+5.7}_{-3.9}$	$9.7^{+3.1}_{-2.2}$	<0.032	<0.56	–	>1.73	$1.87^{+0.14}_{-0.13}$
NGC 4710	$6.3^{+0.9}_{-0.9}$	$6.5^{+1.0}_{-0.9}$	$0.061^{+0.010}_{-0.010}$	$0.39^{+0.06}_{-0.06}$	$1.59^{+0.24}_{-0.20}$	$4.10^{+0.82}_{-0.71}$	$1.32^{+0.04}_{-0.04}$
NGC 5866	$6.2^{+0.9}_{-0.9}$	$4.3^{+0.7}_{-0.7}$	$0.059^{+0.010}_{-0.010}$	$0.36^{+0.07}_{-0.06}$	$1.48^{+0.32}_{-0.25}$	$4.10^{+1.00}_{-0.80}$	$3.07^{+0.13}_{-0.13}$
NGC 6014	$9.0^{+2.3}_{-1.8}$	$6.7^{+1.1}_{-1.1}$	$0.040^{+0.011}_{-0.011}$	$0.36^{+0.13}_{-0.11}$	>1.46	>5.51	$1.58^{+0.10}_{-0.09}$
NGC 7465	$17.9^{+5.7}_{-4.0}$	$18.1^{+2.8}_{-2.7}$	$0.015^{+0.004}_{-0.004}$	$0.27^{+0.11}_{-0.09}$	$0.44^{+0.13}_{-0.12}$	$1.63^{+0.48}_{-0.44}$	$1.05^{+0.04}_{-0.04}$
UGC 09519	$26.2^{+8.9}_{-6.0}$	$15.1^{+4.6}_{-3.2}$	<0.017	<0.47	<0.72	$1.08^{+0.47}_{-0.34}$	$1.18^{+0.04}_{-0.04}$
PGC 058114	$18.9^{+4.6}_{-3.6}$	$14.4^{+3.1}_{-2.6}$	<0.029	<0.58	<0.85	$1.05^{+0.49}_{-0.31}$	$2.30^{+0.08}_{-0.08}$

is double in diameter to that of the (2–1) transition, so the higher $\mathfrak{R}_{10}$ ratios may indicate that the more extended gas traced by the (1–0) transition is more optically thin in some early-type galaxies. However, the difference in the (1–0) and (2–1) ratios may instead be dominated by the global temperature and density of the molecular gas. Spatially resolved studies will have to determine what drives the higher $\mathfrak{R}_{10}$ compared to $\mathfrak{R}_{21}$ ratios.

The highest $\mathfrak{R}_{10}$ and $\mathfrak{R}_{21}$ ratios for the early-type sample are similar to those of the most extreme starbursts, while the lowest ratios have never before been seen in integrated galaxy measures, matching the very lowest values ever measured in galaxy discs (Tan et al. 2011). As mentioned above, spirals have radial gradients in $\mathfrak{R}_{10}$, the value generally decreasing with radius in the disc (Paglione et al. 2001; Tan et al. 2011), although it can have local maxima within spiral arms or intense star-forming regions (Schinnerer et al. 2010; Tan et al. 2011). In general, high $\mathfrak{R}_{10}$ ratios seem to signal more active star formation by tracing the diffuse gas created by feedback processes. The majority of early-type galaxies have $\mathfrak{R}_{10}$ ratios similar to those of spirals (5–20), with NGC 1222, NGC 1266 and UGC 09519 being exceptions at the high end and NGC 4526, NGC 4459 and NGC 3665 being exceptions at the low end.

Figs 4(a) and 5(a) show how the $\mathfrak{R}_{10}$ ratio varies with several galaxy properties, Fig. 4(a) focusing on ISM properties and environment and Fig. 5(a) focusing on stellar properties. The galaxy with a significant molecular outflow, NGC 1266, is identified in each plot with a circle and will be discussed separately. At the top of each plot, the Spearman rank correlation coefficient and the probability that the null hypothesis (no correlation) is true are given. Low probabilities for the null hypothesis (we take 'low' to be less than 0.03) suggest the data are correlated. The dust morphology has two discrete categories (disc and filament), so the null hypothesis is that the sample means are the same. We evaluate this probability by Welch's *t*-test (similar to the Student *t*-test but not assuming that the sample variances are the same).

By the above measures, $\mathfrak{R}_{10}$ is correlated with the molecular-to-atomic gas ratio (atomic gas measured by H I emission), the dust temperature, M_K and the single stellar population (SSP) derived age. The $\mathfrak{R}_{10}$ ratios of the galaxies with dust discs are also significantly different than those of galaxies with filamentary dust. On the other hand, no significant correlation is found with the [O III]/Hβ emission line ratio (a measure of the ionized gas excitation), local environment (Σ_3), SSP-derived metallicity or alpha-element enhancement, or specific stellar angular momentum ($\lambda_R/\sqrt{\epsilon_e}$).

Of course, not all of these parameters are independent. Stellar luminosity (or mass) is known to positively correlate with the SSP-derived age, metallicity and alpha-element enhancement (Trager et al. 2000; Thomas et al. 2005; McDermid et al., in preparation). The bright-CO selection criterion results in a relation between stellar mass and gas fraction such that galaxies with higher stellar mass have low gas fraction and vice versa. The galaxies with higher gas fractions tend to be those that are interacting, with lower molecular-to-atomic gas ratios, filamentary dust morphologies and higher dust temperatures, while the low gas-fraction galaxies are more molecular, with settled and colder dust discs (see Table 1). We note that low mass galaxies with low gas fractions (and settled dust morphologies and low dust temperatures) do exist among the 56 CO-detected ATLAS^{3D} galaxies. Observing such galaxies will help separate some of these currently degenerate parameters. To proceed with the current sample, we draw from the most plausible of relations, supported by previous work on late-type galaxies.

It has long been known that $\mathfrak{R}_{10}$ directly correlates with the dust temperature in spiral and starburst galaxies (e.g. Young & Sanders 1986; Aalto et al. 1995). The explanation proposed is that hot dust temperatures signal more efficient star formation (more UV photons impinging on a given quantity of dust), which in turn may produce optically thin molecular outflows or a hot, diffuse component of molecular gas through radiative feedback. In either case, higher $\mathfrak{R}_{10}$ ratios result.

© 2012 The Authors, MNRAS **421,** 1298–1314
Monthly Notices of the Royal Astronomical Society © 2012 RAS

All of the sample galaxies with high $\mathfrak{R}_{10}$ ratios have filamentary dust structure, indicating an unsettled ISM. Signs of interaction are also often visible, either in stellar light (Paper II; Duc et al. 2011, hereafter Paper IX) or in tails of atomic gas (Serra et al. 2012).

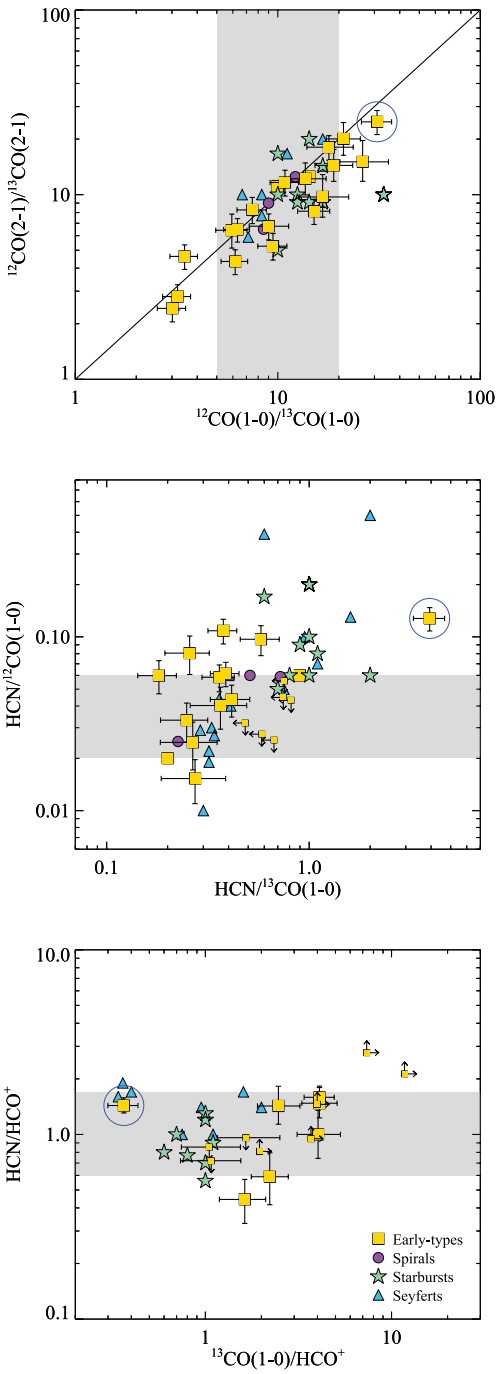

Figure 3. Molecular line ratio diagrams. Early-type galaxies are represented by yellow squares with error bars or upper or lower limits. Spirals, starbursts and Seyfert nuclei are portrayed by purple circles, green stars and blue triangles, respectively (Krips et al. 2010). The grey band highlights the region occupied by spirals from Paglione et al. (2001) in the top plot, spirals from Gao & Solomon (2004a) in the middle plot, and GMCs in M31 (Brouillet et al. 2005) in the bottom plot. The band reflects the fact that the ratio along one axis is not yet well constrained by literature data. NGC 1266, a sample galaxy with a molecular outflow, is identified by blue circles. Cen A is represented by yellow squares without error bars.

However, unlike the direct relation between $\mathfrak{R}_{10}$ and f_{60}/f_{100} seen in Young & Sanders (1986) and Aalto et al. (1995), a number of the early-type galaxies with high $\mathfrak{R}_{10}$ do not have particularly warm dust (IC 1024, NGC 4694, NGC 7465 and UGC 09519). These galaxies are interacting or accreting, but do not (currently) have starburst or nuclear activity substantially heating their dust. For these galaxies, the low optical depth in ^{12}CO(1–0) must be attributed to unsettled gas as opposed to feedback from intense star formation. Indeed, interacting galaxies have been observed to have increased gas velocity dispersions (Irwin 1994; Elmegreen et al. 1995), which would allow for a decreased optical depth in ^{12}CO(1–0).

Thus, the $\mathfrak{R}_{10}$ ratio seems driven to higher values by gas-rich interactions (major mergers, minor mergers or tidal gas capture) and/or feedback from starburst activity. The gas-rich interactions tend to have large amounts of atomic gas involved, thus explaining the correlation with the molecular-to-atomic gas ratio. Dust temperatures of these galaxies are middle to high, never very low. The strong apparent correlation with K-band luminosity may be due to our sample selection, since we have no high mass, high gas-fraction (generally interacting) galaxies or low mass, low gas-fraction (generally settled) galaxies. Similarly, the strong trend with SSP age may be tied to the biased gas fraction because SSP age is very sensitive to the fraction of young to old stars (which is presumably higher in high gas-fraction galaxies). As mentioned above, including low mass, low gas-fraction galaxies in future work will allow us to see if either galaxy mass or SSP age affects the $\mathfrak{R}_{10}$ line ratio.

In the fourth panel of Fig. 4(a), the eye is drawn to a correlation between [O III]/Hβ, although the Spearman correlation coefficient reveals this is not particularly likely. Indeed, it is hard to state a connection: high $\mathfrak{R}_{10}$ galaxies shy away from the lowest values of [O III]/Hβ while low $\mathfrak{R}_{10}$ galaxies have middle-valued ratios. Coupled with another optical emission line ratio such as [N II]/Hα or [S II]/Hα, [O III]/Hβ is frequently used to distinguish H II-region photoionization from shock ionization or from a power-law continuum source such as an AGN. Unfortunately, without the second line ratio, the values observed for our galaxies are degenerate. Thus, the lack of a clear correlation may be due to various ionization sources which are differently (or not) related to molecular gas properties.

Some relation also looks possible for $\mathfrak{R}_{10}$ and Σ_3, mostly driven by galaxies at high local environmental densities having low $\mathfrak{R}_{10}$ values. These are all galaxies that are in the Virgo cluster or the centre of their group. It is possible that in these galaxies, the molecular gas is additionally pressure confined by the hot intragroup or intracluster medium and so has such high optical depth. But more galaxies are needed to rule in such a scenario.

We have suggested that either stellar feedback and/or ongoing accretion of cold gas leads to more optically thin molecular gas and higher $\mathfrak{R}_{10}$ ratios. However, chemical effects may also be able to explain such relations. ^{13}C is a secondary product of nucleosynthesis and should build up in abundance relative to ^{12}C as a stellar population ages and returns material to the ISM. Interactions may bring less enriched material into galaxies, with presumably less ^{13}C, explaining the higher $\mathfrak{R}_{10}$ ratio seen in these systems. Chemical fractionation due to isotopic ion exchange towards ^{13}CO and away from ^{12}CO may also cause the trend with f_{60}/f_{100}; at lower temperatures the lower energy ^{13}CO will be more strongly preferred. If the majority of molecular gas is at low temperatures in the more settled galaxies, then this option could also be responsible for the observed trends. Ratios involving HCN and HCO$^+$ help disentangle these options in the next sections.

© 2012 The Authors, MNRAS **421,** 1298–1314
Monthly Notices of the Royal Astronomical Society © 2012 RAS

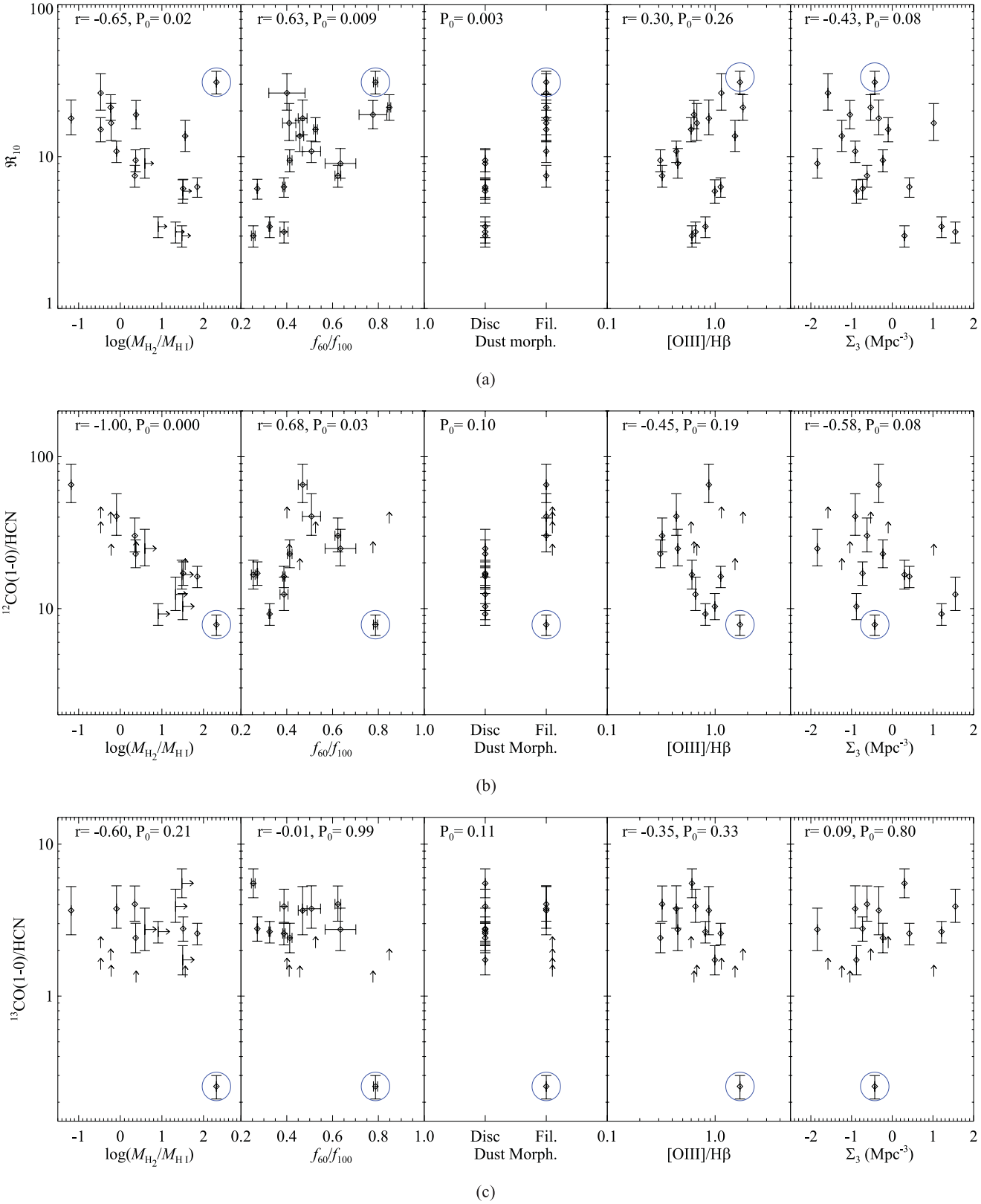

Figure 4. Molecular line ratios against ISM properties and environment (from left to right): (1) molecular-to-atomic gas ratio; (2) f_{60}/f_{100} ratio of *IRAS* fluxes (a dust temperature proxy); (3) dust morphology (disc or filamentary; from Paper II); (4) median [O III]/Hβ emission line ratio (a measure of the ionized gas excitation; from Sarzi et al., in preparation); and (5) ρ_{10} (a measure of the local galaxy density; from Paper VII). From top to bottom, the molecular ratios are (a) $\mathfrak{R}_{10}$, (b) ^{12}CO(1–0)/HCN and (c) ^{13}CO(1–0)/HCN. NGC 1266 is highlighted with a circle. The Spearman rank correlation coefficient ('r') and the probability that the null hypothesis ('P_0', no correlation) is true are given at the top of each plot.

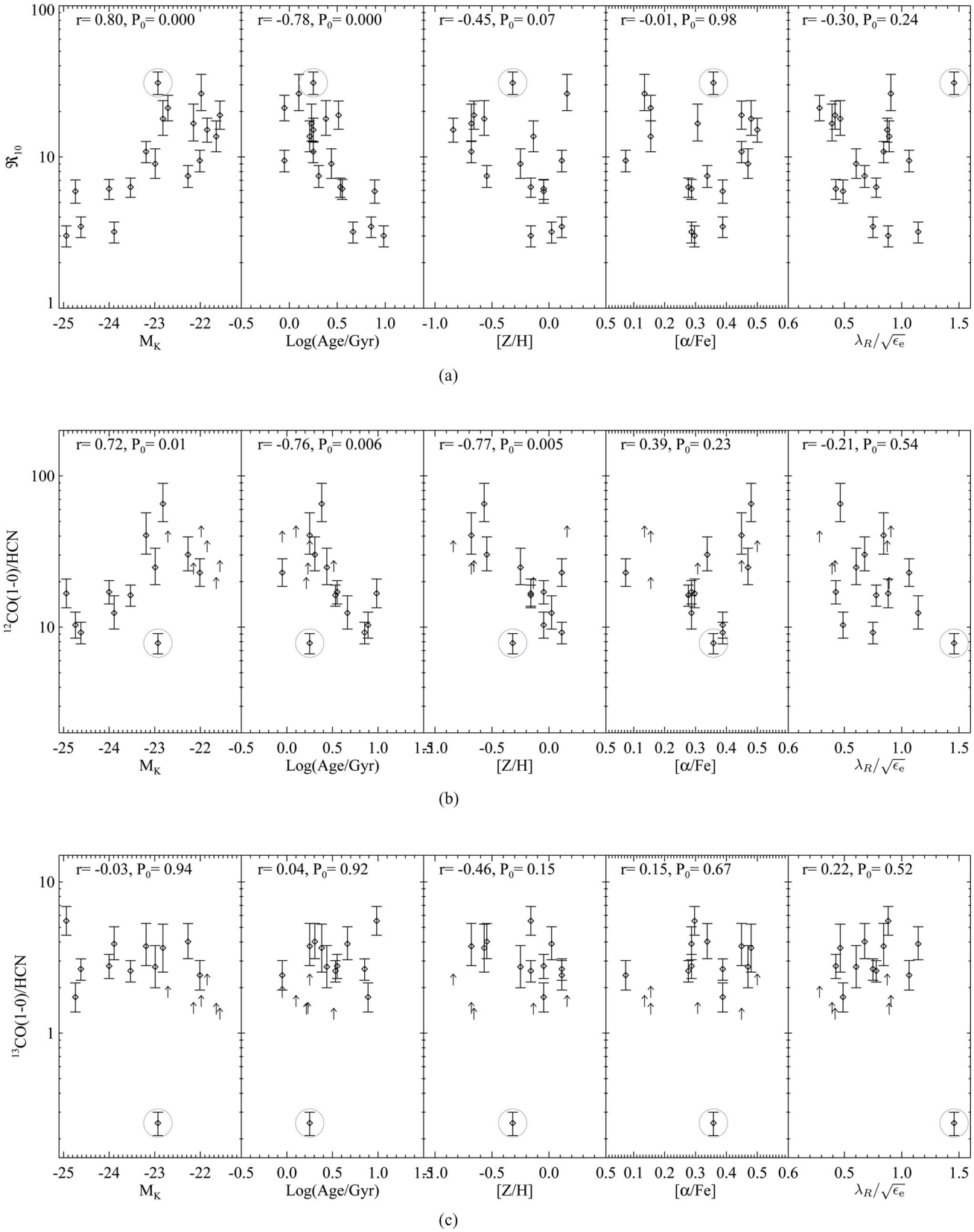

Figure 5. Molecular line ratios against stellar properties (from left to right): (1) absolute *K*-band magnitude, SSP best-fit; (2) age; (3) metallicity; (4) alpha-element abundance (McDermid et al., in preparation); and (5) specific stellar angular momentum normalized by ellipticity (Paper II). From top to bottom, the molecular ratios are (a) $\mathfrak{R}_{10}$, (b) ^{12}CO(1–0)/HCN and (c) ^{13}CO(1–0)/HCN. NGC 1266 is highlighted with a circle. The Spearman rank correlation coefficient ('*r*') and the probability that the null hypothesis ('P_0', no correlation) is true are given at the top of each plot.

© 2012 The Authors, MNRAS **421,** 1298–1314
Monthly Notices of the Royal Astronomical Society © 2012 RAS

We note that three of the early-type galaxies have extremely low $\mathfrak{R}_{10}$ and $\mathfrak{R}_{21}$ ratios, at the limit seen in spiral galaxy discs: NGC 3665, NGC 4459 and NGC 4526. A $\mathfrak{R}_{10}$ minimum value of 3.3 was reported in Tan et al. (2011), but spiral discs generally have $\mathfrak{R}_{10}$ values above 5 (Young & Sanders 1986; Paglione et al. 2001; Schinnerer et al. 2010). The values observed here indicate that the gas in these three galaxies is either less affected by star formation feedback (remaining very optically thick and/or fractionated towards ^{13}CO) or is more enriched with ^{13}C.

4.2.2 HCN

For HCN, we consider ratios with both ^{12}CO(1–0) and ^{13}CO(1–0) (see Table 4). HCN/^{12}CO(1–0) varies by a factor of about 7, from 0.015 to 0.108, while HCN/^{13}CO(1–0) varies by only a factor ≈3 from 0.18 to 0.58, if NGC 1266 is excluded (because of its unique properties associated with its molecular outflow). Our early-type galaxies mostly lie within the HCN/^{12}CO(1–0) range of normal spirals indicated by the grey band in Fig. 3, based on the galaxies of Gao & Solomon (2004a) with FIR luminosity $L_{\rm FIR} < 10^{11}$ L$_\odot$ (thus below the LIRG luminosity threshold). The three galaxies above the grey band are NGC 3607, NGC 4459 and NGC 4526. These three galaxies were also low in $\mathfrak{R}_{10}$ and $\mathfrak{R}_{21}$, signalling that it may be their weakness in ^{12}CO that is the shared trait between the two ratios. NGC 7465 lies below the grey band; it is a galaxy with high $\mathfrak{R}_{10}$ and $\mathfrak{R}_{21}$. Few spirals have measured HCN/^{13}CO(1–0) ratios, but the early-types definitely have HCN/^{13}CO(1–0) ratios lower than starbursts (even those with high starburst-like $\mathfrak{R}_{10}$ ratios), while they overlap with approximately half of the Seyfert nuclei.

We plot the inverse of these ratios [thus ^{12}CO(1–0)/HCN and ^{13}CO(1–0)/HCN] against the same galactic properties as before to make plots with the same orientation as for $\mathfrak{R}_{10}$ (Figs 4b,c and 5b,c). Again ignoring NGC 1266, very similar trends to those of $\mathfrak{R}_{10}$ are seen with ^{12}CO(1–0)/HCN, although the lower number of galaxies (only 12 detected in HCN) makes it easier for the null hypothesis of no correlation to be accepted. Correlations with the molecular-to-atomic gas ratio, dust temperature, SSP age and M_K are still significant. A correlation with stellar metallicity is also shown to be likely, but would probably not be if the one lower limit at high Z were included. For the ^{13}CO(1–0)/HCN ratio, no correlation is seen with any galaxy parameter.

In the ^{12}CO(1–0)/HCN ratio, there is no difference in the carbon isotope, so the continued presence of most of the trends observed with $\mathfrak{R}_{10}$ rules out enhanced ^{13}C abundance as their cause. If ion–exchange reactions leading to fractionation were responsible for the trends with ^{12}CO(1–0)/HCN, inverse relations would be expected for ^{13}CO(1–0)/HCN. As this is not seen, fractionation is also unlikely to explain the observed trends. With both abundance variations and ion–exchange reactions unable to drive the observed trends, a varied average optical depth of ^{12}CO(1–0) is left as the most likely cause.

HCN/^{12}CO(1–0) is frequently used as a dense gas tracer in star-forming galaxies. Gao & Solomon (2004b) find an increased HCN/^{12}CO(1–0) ratio for LIRG and ULIRG galaxies and suggest that gas traced by HCN is more closely tied to star formation than that traced by ^{12}CO(1–0). In Fig. 6, we place our early-type galaxies on a HCN/^{12}CO(1–0) versus $L_{\rm FIR}$ plot along with the late-type galaxies from Gao & Solomon (2004b). The early-type galaxies at low $L_{\rm FIR}$ do not behave as nicely as the late-types, instead they exhibit a wide range of HCN/^{12}CO(1–0) ratios. However, much of this may be due to the optical depth effects in ^{12}CO(1–0) described

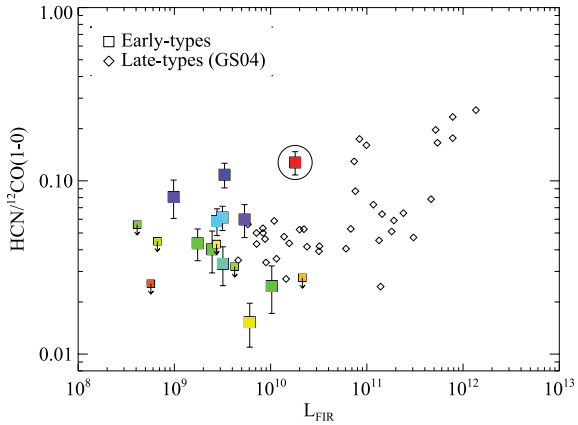

Figure 6. HCN/^{12}CO(1–0) versus FIR luminosity. Early-type galaxies are shown as coloured squares with the colour reflecting their $\mathfrak{R}_{10}$ ratio (blue to red depicts low to high ratios). Late-type galaxies from the Gao & Solomon (2004b) sample are shown as diamonds. NGC 1266 is highlighted by a surrounding circle.

above. We colour-code the early-type galaxies by their $\mathfrak{R}_{10}$ ratio, and as expected if the optical depth of ^{12}CO(1–0) plays a role, galaxies with low $\mathfrak{R}_{10}$ ratios are seen at high HCN/^{12}CO(1–0) and vice versa [a blue colour indicates high HCN/^{12}CO(1–0)]. Thus, HCN/^{12}CO(1–0) is not a good tracer of dense gas fraction in early-type galaxies, HCN/^{13}CO(1–0) should be better. Additionally, we see that NGC 1266 has a high HCN/^{12}CO(1–0) ratio despite its high $\mathfrak{R}_{10}$ ratio. It thus exhibits a dense gas ratio like an LIRG or ULIRG regardless of optical depth considerations. Thus, high dense gas fractions are not limited to galaxies that are extremely bright in the FIR.

If we instead use HCN/^{13}CO(1–0) as a dense gas tracer, we find that there is only about a factor 3 variation in this ratio (ignoring NCC 1266) among the early-type galaxies. Unfortunately, few spiral galaxies have both HCN and ^{13}CO(1–0) measured; only a comparison with a larger spiral sample will really tell whether the early-type galaxies as a population have different dense gas fractions.

4.2.3 HCO$^+$

HCO$^+$(1–0) is detected in 10 of the 18 sample galaxies, including three cases where HCN is not detected (NGC 1222, PGC 058114 and UGC 09519). The HCN/HCO$^+$ ratios for the detected early-type galaxies range from 0.44 (and possibly less) to >2.77. Ratios of 0.66–1.7 are seen in M31 giant molecular clouds (GMCs; Brouillet et al. 2005); this region is shaded in grey in the bottom panel of Fig. 3. Most early-type galaxies are also found within this range, as are most starbursts and Seyferts, although Seyfert nuclei appear biased towards higher and spiral galaxies towards lower HCN/HCO$^+$ ratios (e.g. Krips et al. 2008). As for the ^{13}CO(1–0)/HCO$^+$ ratio, the early-type galaxies have larger ratios than the starbursts (and many of the Seyferts), analogous to the smaller HCN/^{13}CO(1–0) ratios observed. Thus, both ratios agree that early-type galaxies have lower dense gas fractions than starburst (and many Seyfert) galaxies, at least if the latter systems are not dominated by chemical enhancement of HCN and HCO$^+$.

Curiously, two of our galaxies (NGC 3665 and NGC 4526) have quite high HCN/HCO$^+$(1–0) ratios, 2 or higher based on our HCO$^+$ non-detections. These are two of the three galaxies with extremely low $\mathfrak{R}_{10}$ values. The third very low $\mathfrak{R}_{10}$ galaxy (NGC 4459) is also a non-detection in HCO$^+$; its HCN/HCO$^+$ must be above 1.4. None

of these three galaxies has a clear Seyfert nucleus based on optical emission line ratio classification (Ho, Filippenko & Sargent 1997) or a powerful X-ray nucleus, although one (NGC 3665) has conspicuous radio jets that may signal an X-ray bright AGN hidden within. Still, an AGN driving XDR chemistry cannot be the common link between these three galaxies. Instead, the possible low efficiency of star formation in these galaxies may support a lower ionization fraction and thus a smaller abundance of HCO^+ relative to HCN. Information from other molecular gas tracers, such as HNC, will help diagnose if this is the case.

4.3 Molecular gas classes

As mentioned above, early-type galaxies exhibit a variety of molecular line ratios. Here we draw attention to two basic classes: galaxies with settled dust and gas discs and those with unsettled dust and gas.

Galaxies with settled discs include NGC 3032, NGC 3607, NGC 3665, NGC 4459, NGC 4526, NGC 4710, NGC 5866 and NGC 6014. Most also have clearly double-peaked spectra, indicating that the molecular gas distribution extends beyond the turnover of the galaxy's rotation curve (Paper V), and all have more molecular than atomic gas. These galaxies have low $\mathfrak{R}_{10}$ and $\mathfrak{R}_{21}$ values, in three cases strikingly low (below 3). They also have high HCN/^{12}CO(1–0) ratios, consistent with the idea that they are very optically thick in ^{12}CO(1–0). Many also have high (>1.4) HCN/HCO^+(1–0) ratios.

Within this set of settled gas discs, we find that those with the greatest K-band luminosities have the lowest $\mathfrak{R}_{10}$, $\mathfrak{R}_{21}$ and ^{12}CO(1–0)/HCN ratios. If these galaxies also have the least efficient star formation (as predicted by morphological quenching for galaxies with high bulge-to-disc ratios) then the very optically thick molecular gas in these galaxies might result from reduced mechanical and/or radiative feedback accompanying the less efficient star formation. Another option is that they are generally found in environments where hot gas may confine their molecular gas to a thin (and thus more optically thick) layer.

The second class of galaxies we draw attention to are those with unsettled dust (Paper II), signalling either ongoing gas accretion or a merger: IC 676, IC 1024, NGC 1222, NGC 2764, NGC 4694, NGC 7465 and UGC 09519. Recent work suggests that minor mergers are likely to supply the cold gas to many of the currently star-forming early-type galaxies (Kaviraj et al. 2009), so such signs of accretion are not unexpected. These galaxies generally have more atomic than molecular gas and the atomic gas distributions frequently, although not always, show signs of interaction (Serra et al. 2012). PGC 058114 does not have optical photometry for dust classification, but generally seems to fit in this class. These galaxies all have high $\mathfrak{R}_{10}$ ratios and low HCN/^{12}CO(1–0) ratios (see Fig. 4). Increased turbulence from the interaction, diffuse molecular gas within the significant atomic phase and/or significant radiative or mechanical feedback from a related starburst creates a lower optical depth in these galaxies. This group has a wide spread in dust temperatures.

NGC 4150 may bridge the two classes; recent *Hubble Space Telescope* Wide Field Camera 3 (*HST* WFC3) imaging reveals a dust disc with spiral structure and stellar population analysis suggests a recent (≈1 Gyr) minor merger (Crockett et al. 2011). H I observations show a low-column density cloud of atomic hydrogen, possibly leftover from this minor merger (Morganti et al. 2006). However, the overall molecular-to-atomic gas fraction is quite high, making NGC 4150 more similar to members of the settled disc group. Its molecular line ratios lie in the middle of the ranges we observe. In general, there is likely to be a continuum from highly disordered to settled ISM. Many of the interacting galaxies may have developed or may be developing a disc, and some of the galaxies with discs may not be entirely settled yet.

As mentioned previously, NGC 1266 stands apart in many ways from the other galaxies. It has a massive molecular outflow, discovered during the IRAM 30-m survey of the ATLAS^{3D} galaxies (Alatalo et al. 2011). Here we note its extremely high HCN/^{13}CO(1–0) ratio of 2.7, higher than most starbursts and Seyfert nuclei found in the literature. The interpretation of this ratio as an extremely high dense gas fraction fits with the very high surface density implied by the interferometric ^{12}CO observations. But an increased ionization rate due to X-rays, cosmic rays or very intense far UV emission could also boost the HCN abundance. The clear line profile mismatches suggest spatial variations in the molecular properties or multiple molecular components. The ^{12}CO(2–1), HCN(1–0) and HCO^+(1–0) lines were all fitted with wider Gaussians (FWHM = $154^{+1.4}_{-1.4}$, 152^{+15}_{-13} and 176^{+26}_{-21} km s^{-1}, respectively) than the ^{12}CO(1–0) line (FWHM = 132^{+3}_{-3} km s^{-1}), suggesting that they are more prevalent with respect to ^{12}CO(1–0) in the molecular outflow (which reaches higher velocities). On the other hand, the narrow profiles of both the ^{13}CO(1–0) (FWHM = 94^{+9}_{-10} km s^{-1}) and ^{13}CO(2–1) (FWHM = 106^{+9}_{-8} km s^{-1}) lines indicate reduced emission from the ^{13}CO lines in the outflow. The outflow must therefore have an even higher $\mathfrak{R}_{10}$ ratio and is likely very optically thin, consistent with the large velocity gradient modelling performed in Alatalo et al. (2011) using the ^{12}CO(1–0),^{12}CO(2–1) and ^{12}CO(3–2) transitions. The lack of strong ^{13}CO wings confirms that a typical $X_{\rm CO}$ factor should not be used for the molecular outflow.

5 CONCLUSIONS

Using the IRAM 30-m telescope, we have surveyed the ^{13}CO, HCN and HCO^+ emission of the 18 galaxies with the strongest ^{12}CO emission in the ATLAS^{3D} sample of nearby early-type galaxies. We detect all 18 galaxies in both ^{13}CO(1–0) and ^{13}CO(2–1) transitions, 12/18 in HCN(1–0) and 10/18 in HCO^+(1–0).

Fitting the ^{12}CO(1–0) lines with a double-peak or Gaussian profile and evaluating the reduced χ^2 value, we find that one-third of the galaxies are best fitted by a Gaussian, one-third with a clear double-peak profile and the remaining one-third with a very flat-topped 'double-peak' profile. Two galaxies (NGC 1266 and NGC 5866) have clearly different profiles in the various molecular lines, indicating spatial variations of the molecular gas conditions within the galaxies. Discrepant profiles in a few other galaxies are consistent with pointing offsets. We hypothesize that at higher signal-to-noise ratios, the majority of the line profiles would be found to be intrinsically inconsistent due to changing molecular gas conditions. Higher signal-to-noise single-dish data or interferometric maps in the various lines will allow us to determine if this is indeed the case.

The molecular gas line ratios of early-type galaxies are generally consistent with the ranges observed in spiral galaxies, although we also identify some outliers. In terms of the HCN/^{12}CO(1–0) ratio, often used as a dense gas tracer, we extend the work of Gao & Solomon (2004b) to lower FIR luminosities and find an increased scatter in the ratio, compared to late-type galaxies of similar FIR luminosities. Because of the important effects of the optical depth of ^{12}CO(1–0) seen in the $\mathfrak{R}_{10}$ ratio, we suggest that optical depth may be undermining the use of HCN/^{12}CO(1–0) as a dense gas tracer and instead recommend the use of HCN/^{13}CO(1–0). Unfortunately, few spirals have literature HCN/^{13}CO(1–0) ratios. Determining whether the early-types have significantly different dense gas fractions thus

© 2012 The Authors, MNRAS **421,** 1298–1314
Monthly Notices of the Royal Astronomical Society © 2012 RAS

requires a larger sample of spirals to be observed in both HCN(1–0) and ^{13}CO(1–0).

We compare the molecular gas ratios $\mathfrak{R}_{10}$, ^{12}CO(1–0)/HCN and ^{12}CO(1–0)/HCO$^+$ to several ISM and stellar galaxy properties. $\mathfrak{R}_{10}$ is found to correlate with the molecular-to-atomic gas ratio, dust temperature, dust morphology, absolute *K*-band magnitude and SSP age. ^{12}CO(1–0)/HCN similarly correlates with the molecular-to-atomic gas ratio, dust temperature, absolute *K*-band magnitude and SSP age. The persistence of most $\mathfrak{R}_{10}$ correlations with ^{12}CO(1–0)/HCN rules out abundance variations of ^{13}CO as the driving factor of the relations. No correlation with any of these properties is seen in the ^{13}CO(1–0)/HCN ratio, further ruling out a dominant contribution from ion–exchange fractionation towards ^{13}CO at low temperatures.

With these options removed, a change in optical depth of the ^{12}CO(1–0) line is the best explanation for the correlations we see. Based on the lower molecular-to-atomic gas ratios, unsettled dust and occasionally high dust temperatures, we find that high $\mathfrak{R}_{10}$ and ^{12}CO(1–0)/HCN ratios in early-type galaxies are linked to recent or ongoing interactions and/or starbursts. Both of these processes can naturally account for optically thinner ^{12}CO(1–0) line emission, as interactions are known to be more turbulent and star formation feedback can also produce more turbulence or heat up the molecular gas. Early-type galaxies with settled gas and dust discs tend to have less optically thin molecular gas, along with lower dust temperatures and higher molecular-to-atomic gas mass ratios. The correlations with *K*-band luminosity and SSP age can plausibly be explained by sample selection effects, and further work including less massive early-type galaxies with settled gas and dust discs is required before conclusions are reached.

A set of outliers with low $\mathfrak{R}_{10}$ and $\mathfrak{R}_{21}$, high HCN/^{12}CO(1–0) and only upper limits to their HCN/HCO$^+$ ratios are identified. These galaxies may have particularly stable molecular gas which remains very optically thick in ^{12}CO or have their molecular gas confined to a thin layer by hot gas pressure. NGC 1266, a galaxy with a molecular outflow, also stands apart from both spirals and the rest of the early-type sample. Its HCN/^{13}CO(1–0) and ^{13}CO(1–0)/HCO$^+$ ratios suggest that it has a very high dense gas fraction, but its high $\mathfrak{R}_{10}$ and $\mathfrak{R}_{21}$ values simultaneously suggest that much of its ^{12}CO emission is optically thin. This combination of ratios is seen in some other extremely active starburst or Seyfert galaxies.

ACKNOWLEDGMENTS

AC would like to thank Suzanne Aalto and Ron Snell for useful discussions during the preparation of this work as well as Leslie Sage and Gary Welch for providing ^{12}CO(1–0) and ^{12}CO(2–1) data for two sample galaxies.

This work was supported by the rolling grants 'Astrophysics at Oxford' PP/E001114/1 and ST/H002456/1 and visitors grants PPA/V/S/2002/00553, PP/E001564/1 and ST/H504862/1 from the UK Research Councils. EB thanks John Fell OUP Research Fund, ref 092/267. MC acknowledges support from a Royal Society University Research Fellowship. RLD acknowledges travel and computer grants from Christ Church, Oxford, and support from the Royal Society in the form of a Wolfson Merit Award 502011.K502/jd. RLD also acknowledges the support of the ESO Visitor Programme which funded a three-month stay in 2010.

FB acknowledges support from the European Research Council through grant ERC-StG-257720.

SK acknowledges support from the Royal Society Joint Projects Grant JP0869822.

RMM is supported by the Gemini Observatory, which is operated by the Association of Universities for Research in Astronomy, Inc., on behalf of the international Gemini partnership of Argentina, Australia, Brazil, Canada, Chile, the United Kingdom and the United States of America.

TN and MBois acknowledge support from the DFG Cluster of Excellence 'Origin and Structure of the Universe'.

MS acknowledges support from a STFC Advanced Fellowship ST/F009186/1.

NS and TAD acknowledge support from an STFC studentship.

MBois has received, during this research, funding from the European Research Council under the Advanced Grant Program Number 267399-Momentum.

The authors acknowledge financial support from ESO. The research leading to these results has received funding from the European Community's Seventh Framework Programme (/FP7/2007-2013/) under grant agreement No. 229517.

REFERENCES

Aalto S., Booth R. S., Black J. H., Johansson L. E. B., 1995, A&A, 300, 369
Alatalo K. et al., 2011, ApJ, 735, 88
Brouillet N., Muller S., Herpin F., Braine J., Jacq T., 2005, A&A, 429, 153
Cappellari M. et al., 2011a, MNRAS, 413, 813 (Paper I)
Cappellari M. et al., 2011b, MNRAS, 416, 1680 (Paper VII)
Combes F., Young L. M., Bureau M., 2007, MNRAS, 377, 1795
Crocker A. F., Bureau M., Young L. M., Combes F., 2008, MNRAS, 386, 1811
Crocker A. F., Bureau M., Young L. M., Combes F., 2011, MNRAS, 410, 1197
Crockett R. M. et al., 2011, ApJ, 727, 115
Davis T. A. et al., 2011, MNRAS, 414, 968 (Paper V)
Duc P.-A. et al., 2011, MNRAS, 417, 863 (Paper IX)
Eckart A., Cameron M., Rothermel H., Wild W., Zinnecker H., Rydbeck G., Olberg M., Wiklind T., 1990, ApJ, 363, 451
Elmegreen D. M., Kaufman M., Brinks E., Elmegreen B. G., Sundin M., 1995, ApJ, 453, 100
Emsellem E. et al., 2011, MNRAS, 414, 888 (Paper III)
Gao Y., Solomon P. M., 2004a, ApJS, 152, 63
Gao Y., Solomon P. M., 2004b, ApJ, 606, 271
Graciá-Carpio J., García-Burillo S., Planesas P., Colina L., 2006, ApJ, 640, L135
Grossi M. et al., 2009, A&A, 498, 407
Helfer T. T., Blitz L., 1997, ApJ, 478, 233
Ho L. C., Filippenko A. V., Sargent W. L. W., 1997, ApJS, 112, 315
Hubble E. P., 1936, Realm of the Nebulae. Yale Univ. Press, New Haven, CT
Irwin J. A., 1994, ApJ, 429, 618
Jog C. J., Solomon P. M., 1984, ApJ, 276, 127
Juneau S., Narayanan D. T., Moustakas J., Shirley Y. L., Bussmann R. S., Kennicutt R. C., Vanden Bout P. A., 2009, ApJ, 707, 1217
Kaviraj S. et al., 2007, ApJS, 173, 619
Kaviraj S., Peirani S., Khochfar S., Silk J., Kay S., 2009, MNRAS, 394, 1713
Kawata D., Cen R., Ho L. C., 2007, ApJ, 669, 232
Knapp G. R., Kerr F. J., Henderson A. P., 1979, ApJ, 234, 448
Krajnović D. et al., 2011, MNRAS, 414, 2923 (Paper II)
Krips M. et al., 2007, A&A, 468, L63
Krips M., Neri R., García-Burillo S., Martín S., Combes F., Graciá-Carpio J., Eckart A., 2008, ApJ, 677, 262
Krips M., Crocker A. F., Bureau M., Combes F., Young L. M., 2010, MNRAS, 407, 2261
Lepp S., Dalgarno A., 1996, A&A, 306, L21

Markwardt C. B., 2009, in Bohlender D. A., Durand D., Dowler P., eds, ASP Conf. Ser. Vol. 411, Astronomical Data Analysis Software and Systems XVIII. Astron. Soc. Pac., San Francisco, p. 251
Martig M., Bournaud F., Teyssier R., Dekel A., 2009, ApJ, 707, 250
Morganti R. et al., 2006, MNRAS, 371, 157
Paglione T. A. D. et al., 2001, ApJS, 135, 183
Papadopoulos P. P., 2007, ApJ, 656, 792
Paturel G., Theureau G., Bottinelli L., Gouguenheim L., Coudreau-Durand N., Hallet N., Petit C., 2003, A&A, 412, 57
Phillips T. G. et al., 1987, ApJ, 322, L73
Sage L. J., Wrobel J. M., 1989, ApJ, 344, 204
Sage L. J., Welch G. A., Young L. M., 2007, ApJ, 657, 232
Saintonge A. et al., 2011, MNRAS, 415, 61
Sandage A., 1961, The Hubble Atlas of Galaxies. Carnegie Institution, Washington, DC
Schinnerer E., Weiß A., Aalto S., Scoville N. Z., 2010, ApJ, 719, 1588
Scoville N. Z., Solomon P. M., 1974, ApJ, 187, L67
Serra P. et al., 2012, MNRAS, in press
Shapiro K. L. et al., 2010, MNRAS, 402, 2140
Springob C. M., Haynes M. P., Giovanelli R., Kent B. R., 2005, ApJS, 160, 149
Struve C., Oosterloo T. A., Morganti R., Saripalli L., 2010, A&A, 515, A67
Tan Q.-H., Gao Y., Zhang Z.-Y., Xia X.-Y., 2011, Res. Astron. Astrophys., 11, 787
Thomas D., Maraston C., Bender R., Mendes de Oliveira C., 2005, ApJ, 621, 673
Trager S. C., Faber S. M., Worthey G., González J. J., 2000, AJ, 120, 165
van Gorkom J. H., van der Hulst J. M., Haschick A. D., Tubbs A. D., 1990, AJ, 99, 1781
Wang Z., Kenney J. D. P., Ishizuki S., 1992, AJ, 104, 2097
Welch G. A., Sage L. J., 2003, ApJ, 584, 260
Wiklind T., Henkel C., 1989, A&A, 225, 1
Wiklind T., Rydbeck G., 1986, A&A, 164, L22
Wild W., Eckart A., 2000, A&A, 359, 483
Wild W., Eckart A., Wiklind T., 1997, A&A, 322, 419
Young J. S., Sanders D. B., 1986, ApJ, 302, 680
Young J. S., Scoville N. Z., 1991, ARA&A, 29, 581
Young L. M. et al., 2011, MNRAS, 414, 940 (Paper IV)

APPENDIX A: REMAINING SPECTRA

The spectra of the remaining 14 galaxies not shown in Fig. 1 are shown here in Fig. A1.

APPENDIX B: TEST OF LINE PROFILE CONSISTENCY

Here we document how we test for line profile consistency. As the ^{12}CO(1–0) spectra generally have the highest signal-to-noise ratio, so we first fit a single Gaussian and a double-peaked profile to these lines. Our double-peak function is a parabola cut off symmetrically by a steeply declining exponential on either end:

$$f(v) = \begin{cases} T_{\mathrm{mb},w}\mathrm{e}^{-[(v_0-w-v)/15\,\mathrm{km\,s^{-1}}]}, & v < v_0 - w, \\ T_{\mathrm{mb},0} + a(v-v_0)^2, & v_0 - w \le v \le v_0 + w, \\ T_{\mathrm{mb},w}\mathrm{e}^{-[(v-v_0-w)/15\,\mathrm{km\,s^{-1}}]}, & v > v_0 + w. \end{cases}$$

The parabola is a function of the velocity, v, and is centred at v_0, with a cut-off at $v_0 \pm w$ on either side. $T_{\mathrm{mb},0}$ gives T_{mb} at the central velocity, v_0, and the parameter 'a' describes the steepness of the parabola ($a \geq 0$ in order to guarantee a double-peak or flat-topped shape). $T_{mb,w} = T_{\mathrm{mb},0} + aw^2$ is the peak height. Instead of a sharp cut-off from the peaks to zero, which leads to fitting problems, a steep exponential decay with a decay constant of 15 km s^{-1} is specified on both sides.

The fits were performed with the Interactive Data Language (IDL) package MPFIT (Markwardt 2009). The reduced χ^2 values for the Gaussian and double-peak fits to the ^{12}CO(1–0) spectra are listed for each galaxy in Table B1. 7/18 galaxies are best fitted by a single Gaussian, 6/18 by a true double-peak profile and 5/18 by a flat-topped profile ($a = 0$). For most galaxies, this fit-based classification agrees with the by-eye classification in Davis et al. (2011, hereafter Paper V).

For all the other transitions of each galaxy, we constrain the type of fit to that which provides the lower χ^2 value in the ^{12}CO(1–0) line. Uncertainties in the fit parameters are then determined by Monte Carlo simulations, adding Gaussian noise to the observed spectra and refitting 1000 times. The distributions of the resulting parameters are not necessarily Gaussian, so we use the equivalent to a 2σ range, containing 95 per cent of the probability. The measured line profiles are considered consistent with each other when the uncertainties on all their parameters (v_0 and σ for the Gaussian, v_0, w and a for the double-peak profile) overlap. We use the ^{12}CO(1–0) profile as a base and compare the other lines to it.

Table B1 lists whether the line profile of each of the other five lines is consistent with that of ^{12}CO(1–0) (1 indicates consistency, 0 inconsistency). We note that consistency here is not that the intrinsic line profiles agree to within a certain measure, but instead that the observed line profiles do not rule out such agreement (i.e. are often of too low signal-to-noise ratio).

APPENDIX C: DERIVATION OF BEAM CORRECTION FACTORS

A single-dish telescope measures an average surface brightness (usually expressed as a temperature) that results from the convolution of its main beam pattern with the sky brightness. The pattern of the main beam is roughly a Gaussian, with a half-power beam width (HPBW) that depends inversely on frequency. Thus, for a given telescope, a lower frequency line is measured over a larger sky region than a higher frequency line. For non-uniform sources, different intensities will be measured over differently sized beams, an effect that is often called 'beam dilution' for central point sources or centrally concentrated sources.

Our data consist of the integrated intensities (i.e. brightness temperatures integrated over specific frequency or velocity ranges) of lines at different frequencies, therefore measured over different beam areas. For HCN(1–0) and HCO$^+$(1–0), the frequencies are so close that the difference in area is small ($\approx$1 per cent) and their ratio can be computed without any correction. However, the difference is significant for all other line ratios. In the worst case, we compare the integrated intensity of HCN(1–0) and HCO$^+$(1–0) in a 27.7-arcsec beam to the integrated intensity of ^{12}CO(1–0) in a 21.3-arcsec beam (a factor of 1.7 in area).

To predict and thus correct the effect of different beam sizes, the structure of the source must be known in the tracer used. Interferometric ^{12}CO(1–0) maps obtained for all sources as part of the ATLAS^{3D} project (Alatalo et al., in preparation) reveal the distribution of this line. Unfortunately, the other lines do not yet have interferometric data. Still, we can perform a first-order correction assuming that the distributions of the other lines are identical to that of ^{12}CO(1–0), within a scaling factor.

For each galaxy and for each transition, we first perform the weighted integration of the interferometric ^{12}CO(1–0) map using a Gaussian with appropriate HPBW as the weighting

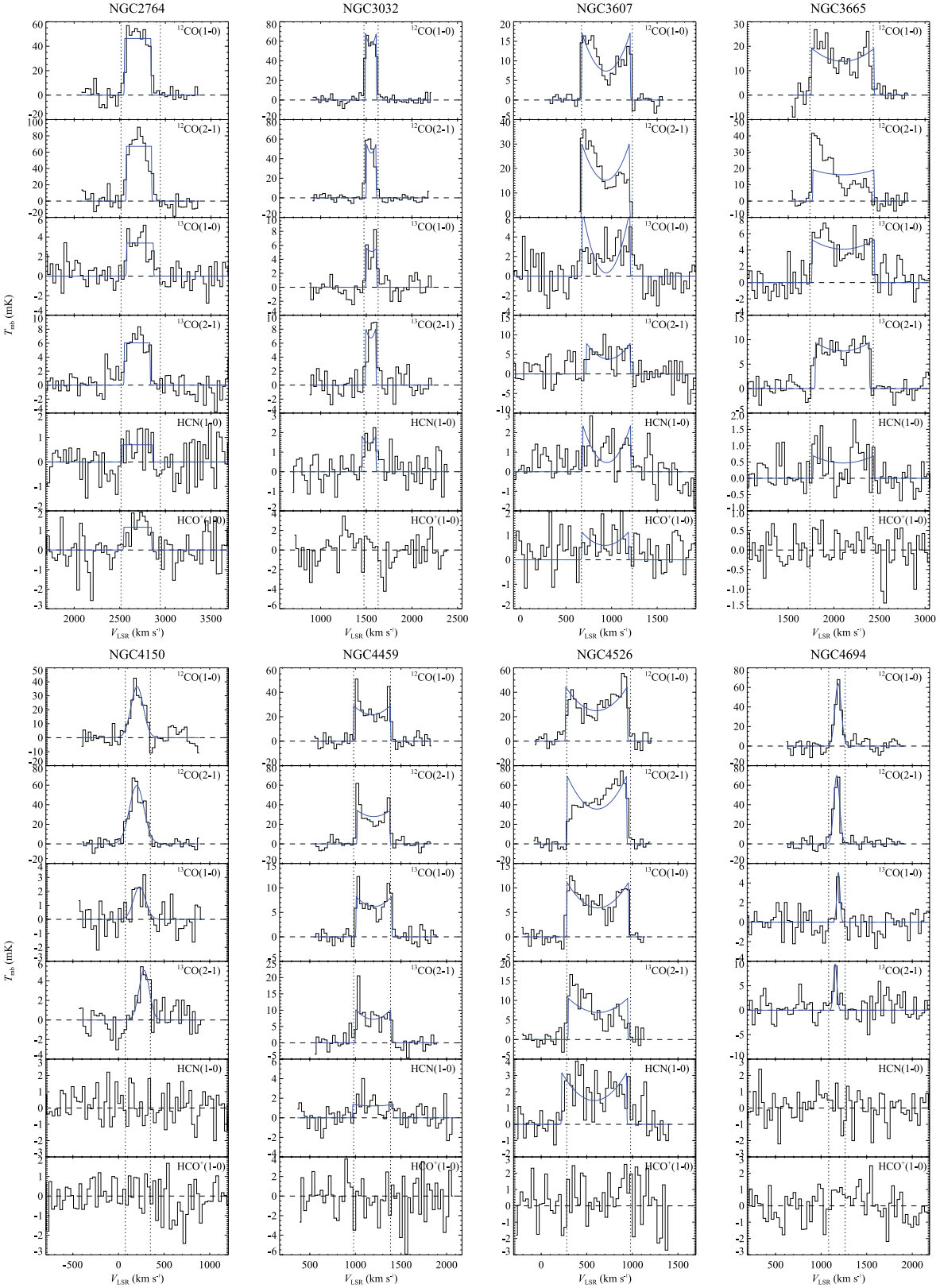

Figure A1. Molecular line spectra from the IRAM 30-m telescope; spectra of the first four galaxies are shown in Fig. 2. The spectra have been binned to a channel width of 30 km s^{-1} and the scale is in main beam temperature (mK). The blue line shows the best-fitting Gaussian or double-peak function (fits are only performed on detected lines). The vertical dashed lines indicate the velocity range integrated over to obtain integrated intensities. Top to bottom: ^{12}CO(1–0), ^{12}CO(2–1), ^{13}CO(1–0), ^{13}CO(2–1), HCN(1–0) and HCO^{+}(1–0). The ^{12}CO(1–0) and ^{12}CO(2–1) data are from Paper IV and Welch & Sage (2003).

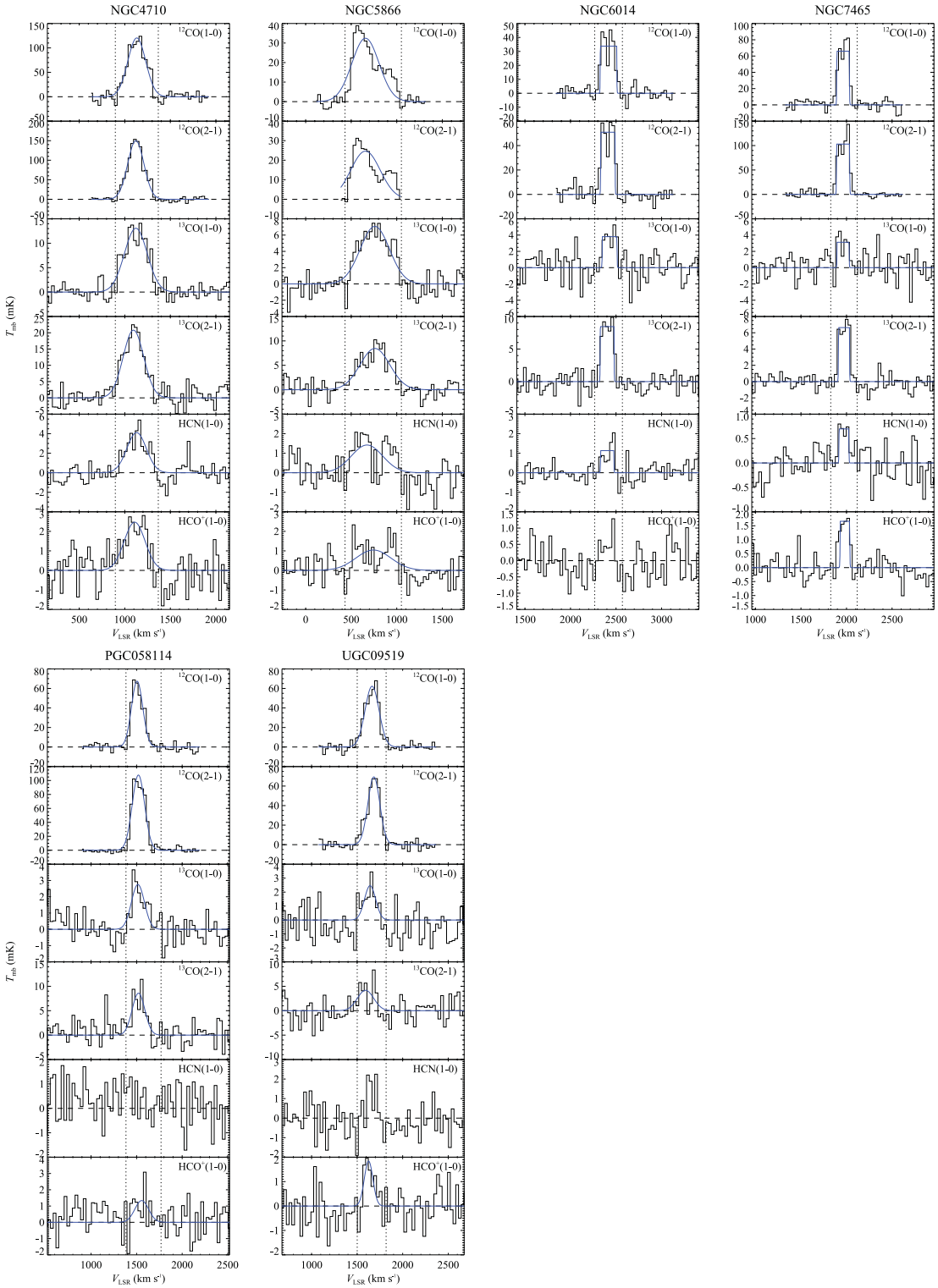

Figure A1 – *continued*

function. The HPBWs we use are determined by the formula HPBW = 2460 arcsec/[ν/GHz]. This results in HPBWs of 27.7, 27.7, 22.3, 21.3, 11.2 and 10.7 arcsec for the HCN(1–0), HCO^+(1–0), ^{13}CO(1–0), ^{12}CO(1–0), ^{13}CO(2–1) and ^{12}CO(2–1) lines, respectively. Then, we divide this spatially integrated flux by the beam area, obtaining an estimate of the integrated intensity of ^{12}CO(1–0) in each differently sized beam. This derived intensity is written as $I^{\rm int}_{\rm HPBW}[^{12}{\rm CO}(1\text{–}0)]$, where the 'int' denotes the interferometric origin and the HPBW is specified in arcseconds. With the assumption that other lines have spatial distributions identical to that of

Table B1. Line profile fits and consistency.

Name	Gaussian χ^2	Double-peak χ^2	Fit	^{12}CO(2–1)	^{13}CO(1–0)	^{13}CO(2–1)	HCN(1–0)	HCO$^+$(1–0)
IC 0676	1.7	1.3	F	1	1	1	1	1
IC 1024	2.9	2.2	F	0	1	1	–	–
NGC 1222	3.7	1.6	D	0	1	1	–	–
NGC 1266	2.0	78.7	G	0	0	0	0	0
NGC 2764	1.8	1.8	F	1	1	1	1	1
NGC 3032	2.1	0.9	D	1	0	1	1	–
NGC 3607	11.4	3.0	D	0	0	0	0	1
NGC 3665	4.0	2.4	D	1	1	1	–	–
NGC 4150	1.1	1.5	G	1	1	0	–	–
NGC 4459	3.3	2.2	D	1	1	1	1	–
NGC 4526	5.8	2.1	D	0	0	0	0	0
NGC 4694	1.0	1.4	G	0	1	1	–	–
NGC 4710	1.9	4.7	G	1	0	0	0	1
NGC 5866	6.8	9.6	G	1	0	0	1	1
NGC 6014	2.5	2.2	F	1	1	1	0	–
NGC 7465	2.0	1.7	F	1	1	1	–	–
UGC 09519	1.6	6.7	G	0	1	1	–	–
PGC 058114	2.4	5.7	G	0	1	1	–	–

Note. The three types of fits denoted in the 'fit' column are a single Gaussian (G), a double-peaked profile (D) or a flat-topped profile (F). The final five columns indicate whether the line specified in the column heading has a profile consistent with the ^{12}CO(1–0) profile (1) or not (0).

Table C1. Integrated intensity correction factors.

Name	$\frac{I^{\rm int}_{21.3\,{\rm arcsec}}[^{12}{\rm CO}(1-0)]}{I^{\rm int}_{22.3\,{\rm arcsec}}[^{12}{\rm CO}(1-0)]}$	$\frac{I^{\rm int}_{10.7\,{\rm arcsec}}[^{12}{\rm CO}(1-0)]}{I^{\rm int}_{11.2\,{\rm arcsec}}[^{12}{\rm CO}(1-0)]}$	$\frac{I^{\rm int}_{21.3\,{\rm arcsec}}[^{12}{\rm CO}(1-0)]}{I^{\rm int}_{27.7\,{\rm arcsec}}[^{12}{\rm CO}(1-0)]}$	$\frac{I^{\rm int}_{22.3\,{\rm arcsec}}[^{12}{\rm CO}(1-0)]}{I^{\rm int}_{27.7\,{\rm arcsec}}[^{12}{\rm CO}(1-0)]}$	$\frac{I^{\rm int}_{10.7\,{\rm arcsec}}[^{12}{\rm CO}(1-0)]}{I^{\rm int}_{21.3\,{\rm arcsec}}[^{12}{\rm CO}(1-0)]}$
IC0676	1.06	1.03	1.35	1.43	1.96
IC1024	1.05	1.02	1.27	1.33	1.62
NGC 1222	1.05	1.02	1.27	1.33	1.63
NGC 1266	1.08	1.05	1.45	1.57	2.60
NGC 2764	1.06	1.05	1.34	1.43	2.28
NGC 3032	1.05	1.02	1.29	1.35	1.62
NGC 3607	1.06	1.03	1.32	1.39	1.92
NGC 3665	1.07	1.05	1.38	1.47	2.32
NGC 4150	1.05	1.04	1.30	1.38	1.97
NGC 4459	1.05	1.02	1.30	1.37	1.60
NGC 4526	1.05	1.03	1.28	1.34	1.71
NGC 4694	1.06	1.04	1.32	1.40	2.01
NGC 4710	1.05	1.02	1.31	1.38	1.68
NGC 5866	1.07	1.05	1.40	1.50	2.47
NGC 6014	1.07	1.04	1.38	1.47	2.29
NGC 7465	1.06	1.03	1.31	1.39	1.89
PGC 058114	1.07	1.07	1.40	1.50	2.24
UGC 09519	1.08	1.08	1.43	1.54	2.54

^{12}CO(1–0) to within a scaling factor, we can then estimate their integrated intensities over different beam sizes. For example, to compute the estimated HCN(1–0) integrated intensity measured over the smaller ^{12}CO(1–0) beam:

$$I'_{21.3\,{\rm arcsec}}({\rm HCN}) = \frac{I^{\rm int}_{21.3\,{\rm arcsec}}[^{12}{\rm CO}(1-0)]}{I^{\rm int}_{27.7\,{\rm arcsec}}[^{12}{\rm CO}(1-0)]}\, I_{27.7\,{\rm arcsec}}({\rm HCN}), \tag{C1}$$

where the prime indicates that this is an estimated, and not directly measured, integrated intensity.

We list the correction factors required for the line ratios we study in Table C1. These have been applied to the ratios listed in Table 4.

This paper has been typeset from a TEX/LATEX file prepared by the author.